Low Energy Nuclear Reactions for Carbon Isotopes, 17F, 17O and light Halo nuclei

Heo Kyongsu, K. S. Choi, W. Y. So, Kyungsik Kim, E. Ha,
K. Hagino, H. Sagawa

Myung-Ki Cheoun (SSU, OMEG)

1. Motivation
1-1. Exotic Light Nuclei
1-2. Low Energy Nuclear Reactions (LENR) for Exotic Nuclei

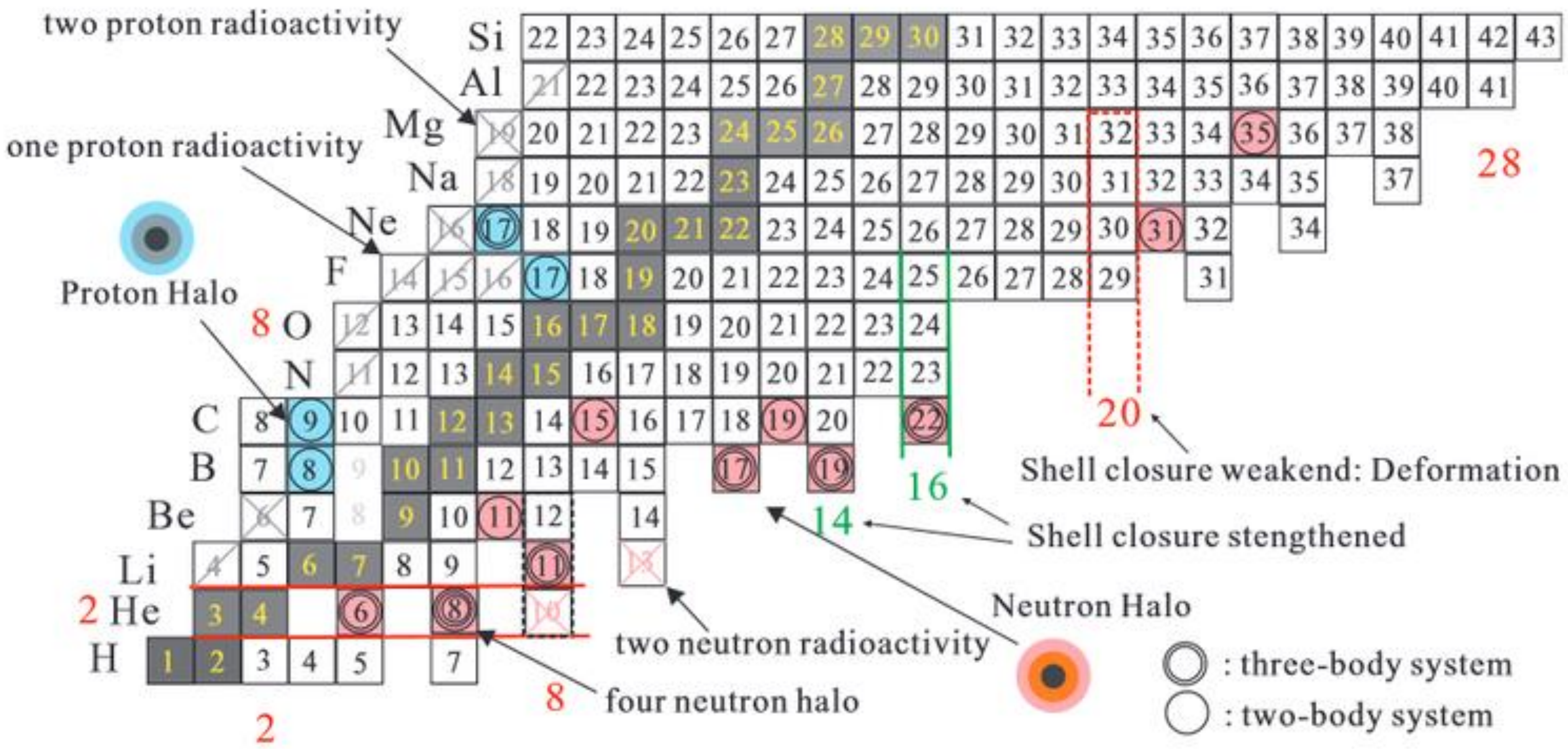
two proton radioactivity
one proton radioactivity
Proton Halo
Si
Al
Mg
Na
Ne
F
O
N
C
B
Be
Li
He
H
28
20
16
14
8
2
Shell closure weakend: Deformation
Shell closure stengthened
Neutron Halo
two neutron radioactivity
four neutron halo
: three-body system
: two-body system

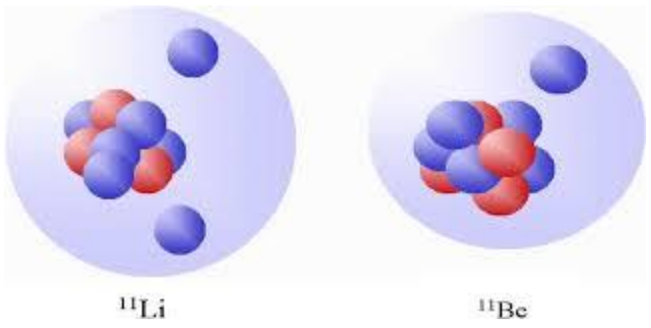
^{11}Li
^{11}Be

- The distribution(rms) of neutron = 2.20 fm
  proton = 2.98 fm
  whole nucleus = 2.72 fm

Light Proton Halo Nuclei

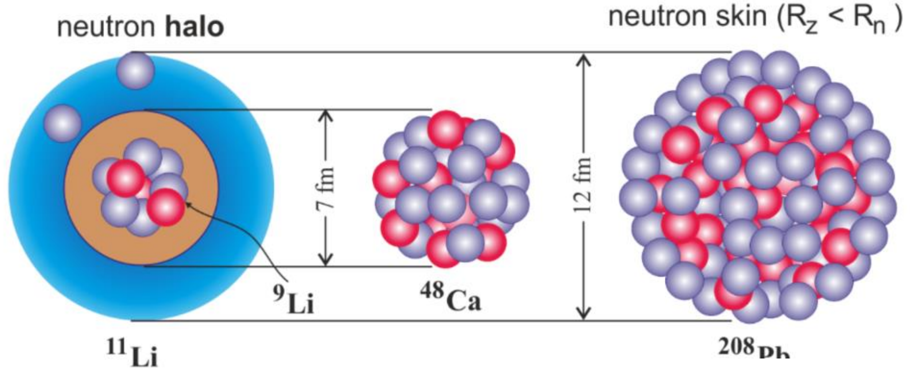

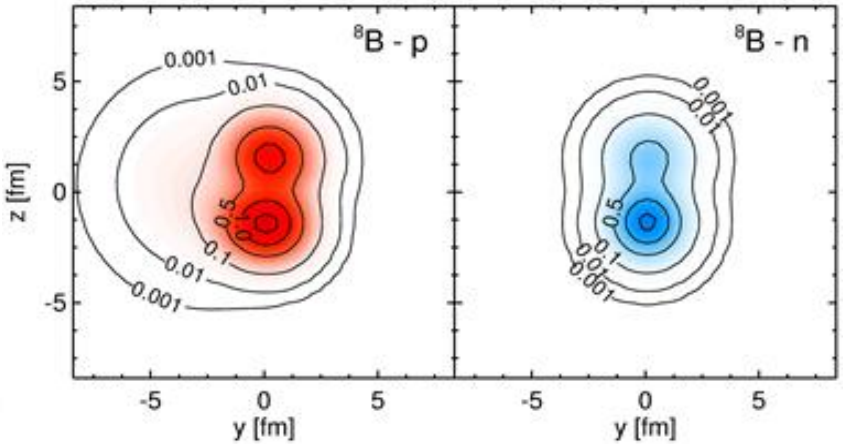

TABLE I. Interaction cross sections (σ_I) in millibarns.

Beam	Target Be	C	Al
^{6}Li	651 ± 6	688 ± 10	1010 ± 11
^{7}Li	686 ± 4	736 ± 6	1071 ± 7
^{8}Li	727 ± 6	768 ± 9	1147 ± 14
^{9}Li	739 ± 5	796 ± 6	1135 ± 7
^{11}Li		1040 ± 60	
^{7}Be	682 ± 6	738 ± 9	1050 ± 17
^{9}Be	755 ± 6	806 ± 9	1174 ± 11
^{10}Be	755 ± 7	813 ± 10	1153 ± 16

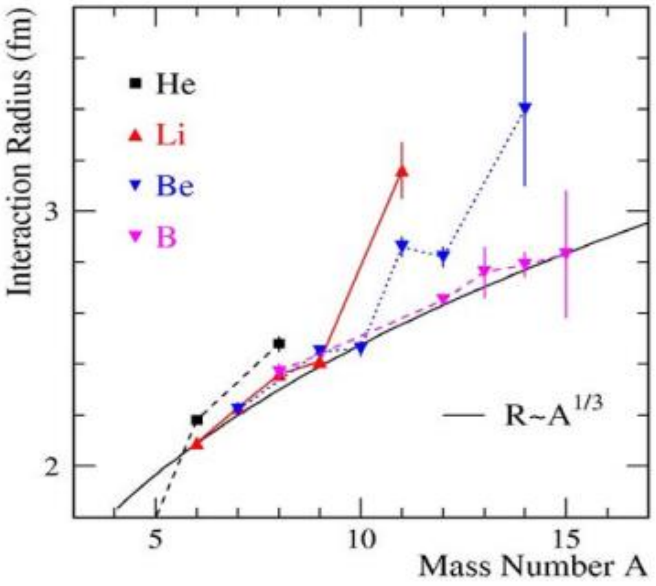

The interaction nuclear radius R_I is defined as

$$\sigma_I(p,t) = \pi[R_I(p) + R_I(t)]^2, \quad (1)$$

where $R_I(p)$ is the projectile radius and $R_I(t)$ is the target radius. The separability of projectile and target radii assumed in the equation was examined by use of σ_I of various projectile-target combinations. Figure 1

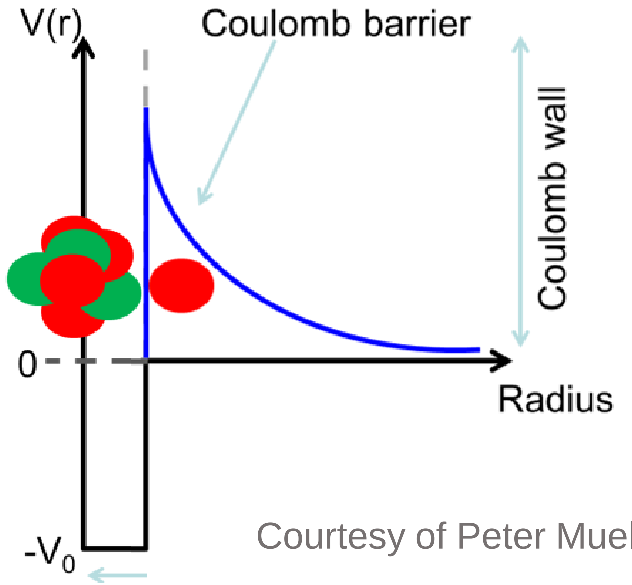

Courtesy of Peter Mueller

Bevalac@LBL, I. Tanihata et al.,
PRL 55 (1985) 2676, PLB 206 (1988) 592

1. Motivation
1-1. Exotic Light Nuclei
1-2. Low Energy Nuclear Reactions (LENR) for Exotic Nuclei

2. LENR for Carbon isotopes
2-1. Quasi-elastic scattering of C isotopes

Submitted to PRC (2022)

	9C	10C	11C	12C
S_n	14.2	21.2	13.1	18.7
S_p	12.9	4.0	8.7	15.9

$$\text{Coulomb barrier} = V_B \approx \frac{Z_p Z_t e^2}{1.44\left(A_P^{\frac{1}{3}} + A_t^{\frac{1}{3}}\right)} = \frac{Z_p Z_t}{\left(A_P^{\frac{1}{3}} + A_t^{\frac{1}{3}}\right)} \text{ [MeV]}$$

~60 MeV

Types of Reactions (in Low energy)

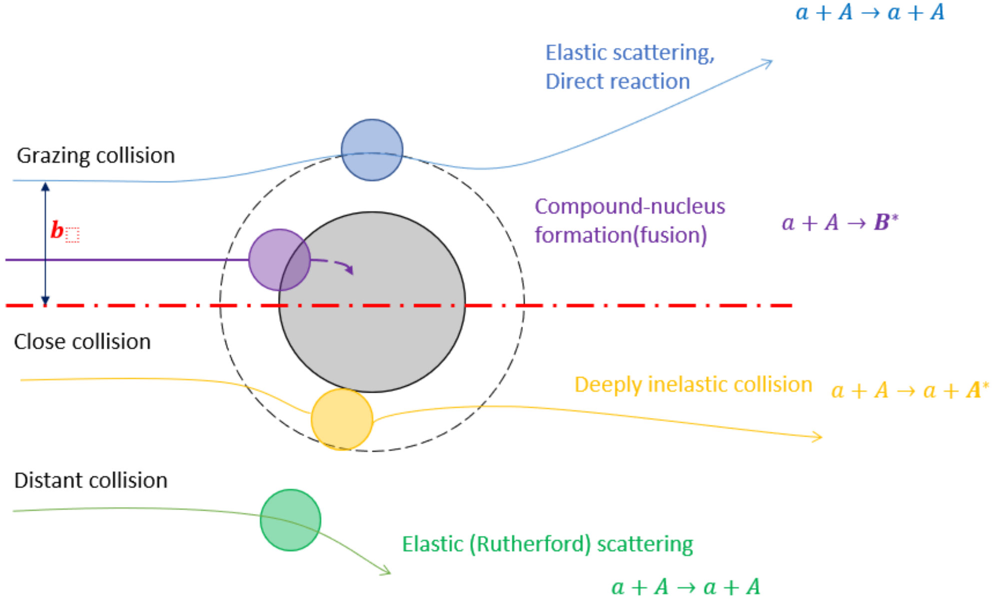

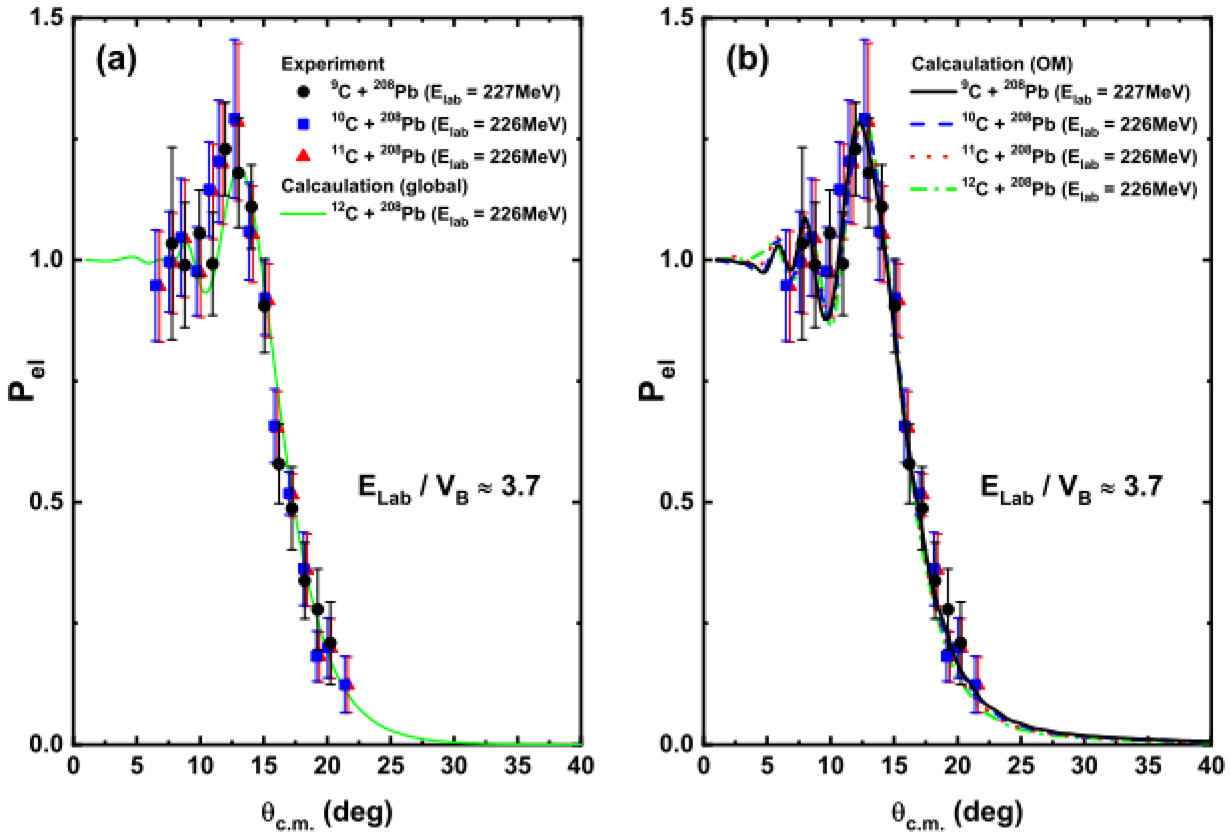

of carbon

FIG. 1: P_{el} ratios for $^{9,10,11,12}C + ^{208}Pb$ system at E_{lab} = 226 MeV or 227 MeV ($E_{lab}/V_B \approx 3.7$). (a) Solid black circles, solid blue squares, and solid red triangles constitute the experimental data for $^{9}C + ^{208}Pb$, $^{10}C + ^{208}Pb$, and $^{11}C + ^{208}Pb$ systems, respectively, accounted from Refs. [18–20]. Solid green line represents theoretical ratios P_{el} for $^{12}C + ^{208}Pb$ system, which were obtained from the global potential parameter set in Table 2 of Ref. [22]. (b) Solid black, dashed blue, dotted red, and dash-dotted green line represent theoretically calculated P_{el} values for $^{9}C + ^{208}Pb$, $^{10}C + ^{208}Pb$, $^{11}C + ^{208}Pb$, and $^{12}C + ^{208}Pb$ systems, respectively, using the optimal parameter set obtained from the OM described in Table I. Refer to the text for detailed explanation.

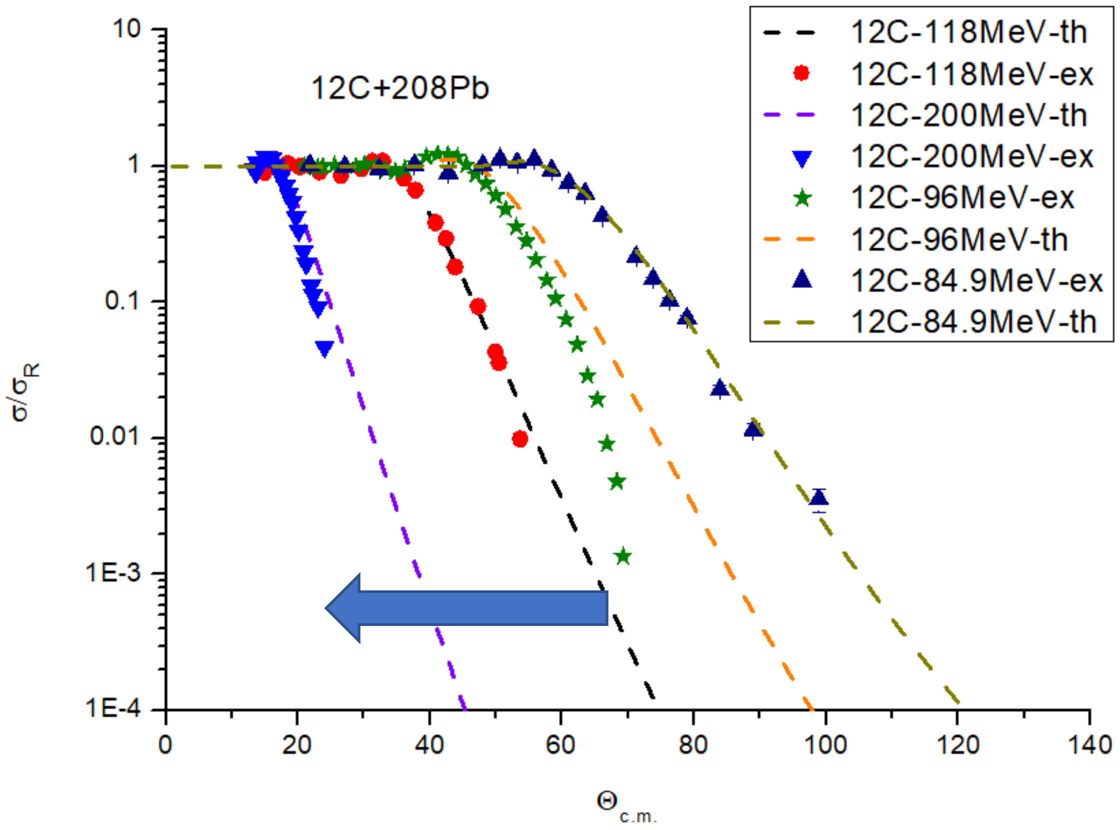

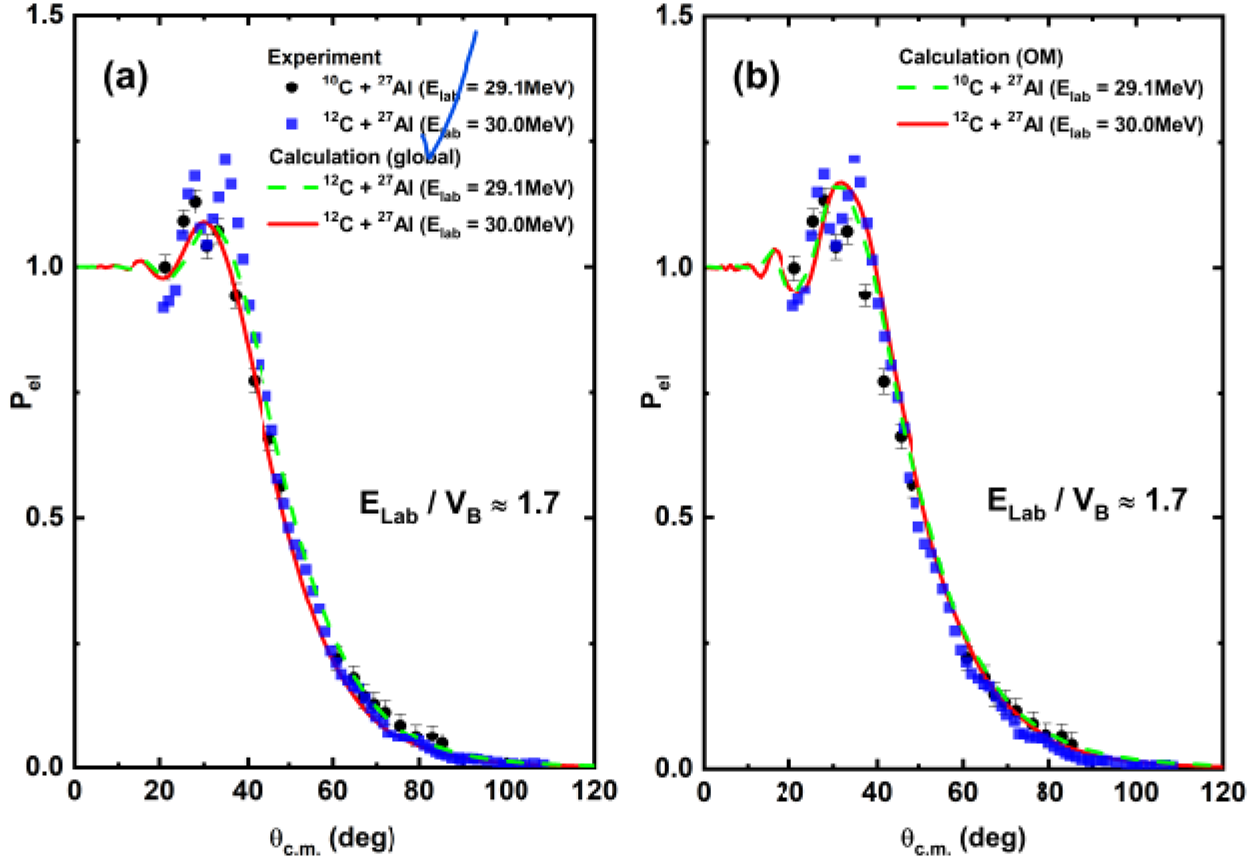

FIG. 2: Same as Fig. 1, but for ^{10,12}C + ^{27}Al systems ($E_{\mathrm{lab}}/V_B \approx 1.7$). (a) Solid black circles and solid blue squares denote experimental data for ^{10}C + ^{27}Al system and ^{12}C + ^{27}Al system, respectively. Experimental data sourced from Refs. [23, 24]. Dashed green and solid red lines denote theoretical P_{el} values for ^{12}C + ^{27}Al system using global potential parameter set in Table 2 of Ref. [22] at $E_{\mathrm{lab}} = 29.1$ and 30.0 MeV, respectively. (b) Solid red and dashed green line represent theoretical P_{el} values for ^{12}C + ^{27}Al and ^{10}C + ^{27}Al systems using the optimal parameter set in Table I obtained from stated OM.

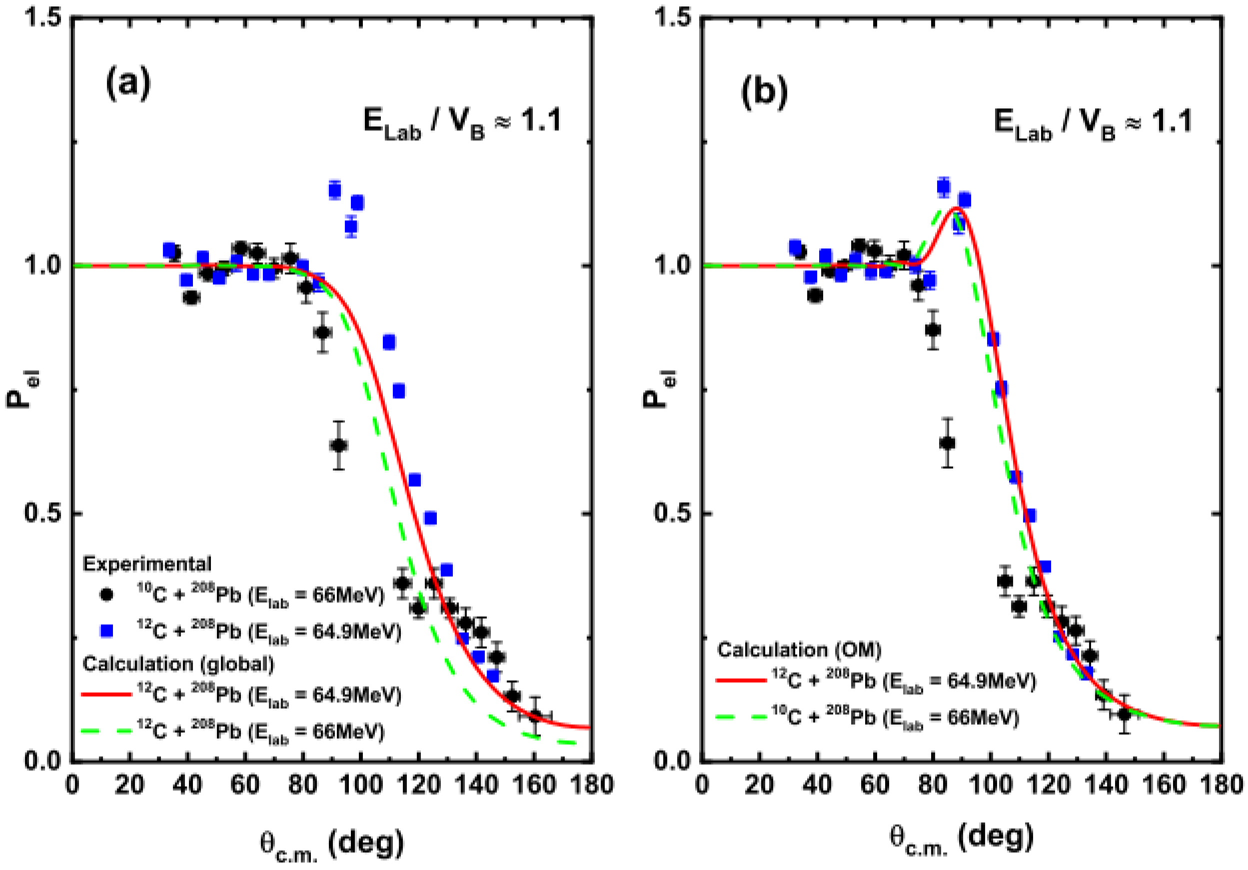

FIG. 3: Similar to that in Fig. 1, but for multiple incident energies ($E_{\rm lab}/V_B \approx 1.1$). (a) Solid black circles and solid blue squares denote the experimental data for ^{10}C + ^{208}Pb system at $E_{\rm lab}$ = 66.0 MeV and ^{12}C + ^{208}Pb system at $E_{\rm lab}$ = 64.9 MeV, respectively. Experimental data acquired from Ref. [16]. Solid red and dashed green lines depict the theoretical calculation of ratios $P_{\rm el}$ for ^{12}C + ^{208}Pb system using the parameter set described in Table 2 of Ref. [22] at $E_{\rm lab}$ = 64.9 and 66.0 MeV, respectively.

III. FORMALISM

To investigate the suppression of the experimental $P_{\rm el}$ values for ^{10}C + ^{208}Pb system, we employed the OM method with the Schrödinger equation as follows [25–27]:

$$[E - T_l(r)]\chi_l^{(+)}(r) = U_{\rm OM}(r)\ \chi_l^{(+)}(r) \tag{1}$$

where $T_l(r)$ and $\chi_l^{(+)}(r)$ represent a kinetic energy operator and a distorted partial wave function expressed as a function of the angular momentum l, respectively. The OM potential $U_{\rm OM}(r)$ in Eq. (1) is composed of the real monopole Coulomb potential $V_{\rm C}(r)$, the energy independent complex bare potential $U(r)$, and the energy dependent complex dynamic polarization potential (DPP) $U_{\rm DPP}(r)$ as follows:

$$\begin{aligned} U_{\rm OM}(r) &= V_{\rm C}(r) - U(r) - U_{\rm DPP}(r) \\ &= V_{\rm C}(r) - U(r) - U_{\rm DR}(r) - U_{\rm F}(r) \\ &= V_{\rm C}(r) - U(r) - U_{\rm inel}(r) - U_{\rm br}(r) - U_{\rm F}(r) \\ &= V_{\rm C}(r) - U(r) - U^{\rm N}_{\rm inel}(r) - iW^{\rm C}_{\rm inel}(r) - U^{\rm N}_{\rm br}(r) - U^{\rm C}_{\rm br}(r) - U_{\rm F}(r). \end{aligned} \tag{2}$$

In Eq. (2), $U(r)$ denotes the bare potential with a volume-type Woods–Saxon potential that is an independent potential for the incident energy of the projectile, expressed as

$$U(r) = (V + iW)\Big[1 + \exp(X_{\rm i})\Big]^{-1}, \quad {\rm i} = V \text{ and } W \tag{3}$$

where $X_{\rm i} = (r - R_{\rm i})/a_{\rm i}$ with $R_{\rm i} = r_{\rm i}\ (A_1^{1/3} + A_2^{1/3})$. In this case, A_1 and A_2 represent the mass numbers for the projectile and target nuclei. Note that the meaning of fusion "V and "W is formed by the real and imaginary components, as further detailed in Sec. IV.

2^+) with the first excitation energy $E_x^{1st} = 3.35$ MeV and B(E2) = 61.5 e^{2}fm^4 [28] below two proton separation energies (S_{2p} = 3.8 MeV). In this study, as the inelastic scattering primarily occurred near the nucleus surface, the nuclear component of the inelastic scattering potential was considered with a differential form of the Woods–Saxon potential, expressed as follows [29]:

$$U^{\rm N}_{\rm inel}(r) = -4\ a^{\rm N}_{\rm i,\ inel}\ \ (V^{\rm N}_{\rm inel} + iW^{\rm N}_{\rm inel})\ \frac{d[1 + \exp(X^{\rm N}_{\rm i,\ inel})]^{-1}}{dr}, \qquad {\rm i} = V \text{ and } W, \tag{4}$$

where $X^{\rm N}_{\rm i,\ inel} = (r - R^{\rm N}_{\rm i,\ inel})/a^{\rm N}_{\rm i,\ inel}$ with $R^{\rm N}_{\rm i,\ inel} = r^{\rm N}_{\rm i,\ inel}\ (A_1^{1/3} + A_2^{1/3})$. As discussed later, among the geometric parameters in Eq. (4), the radius parameters ($R_{\rm i}$) were utilized using

the Coulomb interaction between the projectile and target nucleus. This involves various interactions such as the Coulomb dipole excitation (CDE; E1 transition), CQE (E2 transition), and so forth. As only a single bounded excitation state exists at $J^\pi = 2^+$ for ^{10}C projectile, the Coulomb component of inelastic scattering potential was considered as the Coulomb quadrupole excitation (CQE) interaction by the E2 transition with an imaginary potential, described as follows [30]:

$$W^{\rm C}_{\rm inel.}(r) = \begin{cases} -\left[1 - \frac{2}{7}\left(\frac{r_C}{r}\right)^2 - \frac{1}{21}\left(\frac{r_C}{r}\right)^4\right]\left[1 - \left(\frac{Z_1 Z_2 e^2}{r E_{c.m.}}\right)\right]^{-1/2} \frac{W_P}{r^5} & \text{for } r \geq r_C \\ -\frac{2\sqrt{10}}{3}\ \frac{W_P r^4}{r_C^9} & \text{for } r < r_C \end{cases} \tag{5}$$

the projectile and target nucleus. To explain the breakup effect occurring near the nucleus surface via nuclear interaction, we manipulated the nuclear interaction component of $U_{\mathrm{br}}(r)$ potential as another Wood–Saxon potential with the surface-type constituent as follows:

$$U_{\mathrm{br}}^{\mathrm{N}}(r) = -4\ a_{\mathrm{i,\ br}}^{\mathrm{N}}\ (V_{\mathrm{br}}^{\mathrm{N}} + iW_{\mathrm{br}}^{\mathrm{N}})\ \frac{d[1+\exp(X_{\mathrm{i,\ br}}^{\mathrm{N}})]^{-1}}{dr}, \qquad \mathrm{i} = V \text{ and } W, \tag{7}$$

where $X_{\mathrm{i,\ br}}^{\mathrm{N}} = (r - R_{\mathrm{i,\ br}}^{\mathrm{N}})/a_{\mathrm{i,\ br}}^{\mathrm{N}}$ with $R_{\mathrm{i,\ br}}^{\mathrm{N}} = r_{\mathrm{i,\ br}}^{\mathrm{N}}\ (A_1^{1/3} + A_2^{1/3})$. Subsequently, the Coulomb component of $U_{\mathrm{br}}(r)$ potential can be predicted to contribute to various Coulomb interactions (CDE, CQE , etc.) such as the above-mentioned Coulomb component of the inelastic scattering interaction. However, the contribution of CDE was potentially the largest among them. In particular, as the Coulomb excitation energy (or separation energy; $S_{2p} = 3.8$MeV) associated with the breakup reaction of ^{10}C nuclei by the Coulomb interaction is relatively higher than other weakly bound nuclei such as ^{8}B, ^{11}Li, ^{11}Be, ^{17}F, the separation effect by Coulomb excitation is not substantially dominant. Thus, herein, we considered only the CDE potential as the Coulomb component of the $U_{\mathrm{br}}(r)$ potential. Consequently, the complex CDE potential $U_{\mathrm{br}}^{\mathrm{C}}(r)$ can be expressed as follows [31–34]:

$$U_{\mathrm{br}}^{\mathrm{C}}(r) = \frac{4\pi}{9}\frac{Z_t^2 e^2}{\hbar v}\frac{1}{(r-a_0)^2 r}\int_{\varepsilon_b}^{\infty} d\varepsilon \frac{dB(E1)}{d\varepsilon}\left[g\left(\frac{r}{a_0}-1,\xi\right) + i f\left(\frac{r}{a_0}-1,\xi\right)\right] \tag{8}$$

with

$$f\left(\frac{r}{a_0}-1,\xi\right) = 4\xi^2\left(\frac{r}{a_0}-1\right)^2 \exp(-\pi\xi)\ K_{2i\xi}''\left[2\xi\left(\frac{r}{a_0}-1\right)\right],$$

where a_0 indicate the distance of the closest approach in a head-on collision and $B(E1)$ represents the dipole electric transition strength, respectively. Moreover, $g(\frac{r}{a_0}-1,\xi)$ and K''

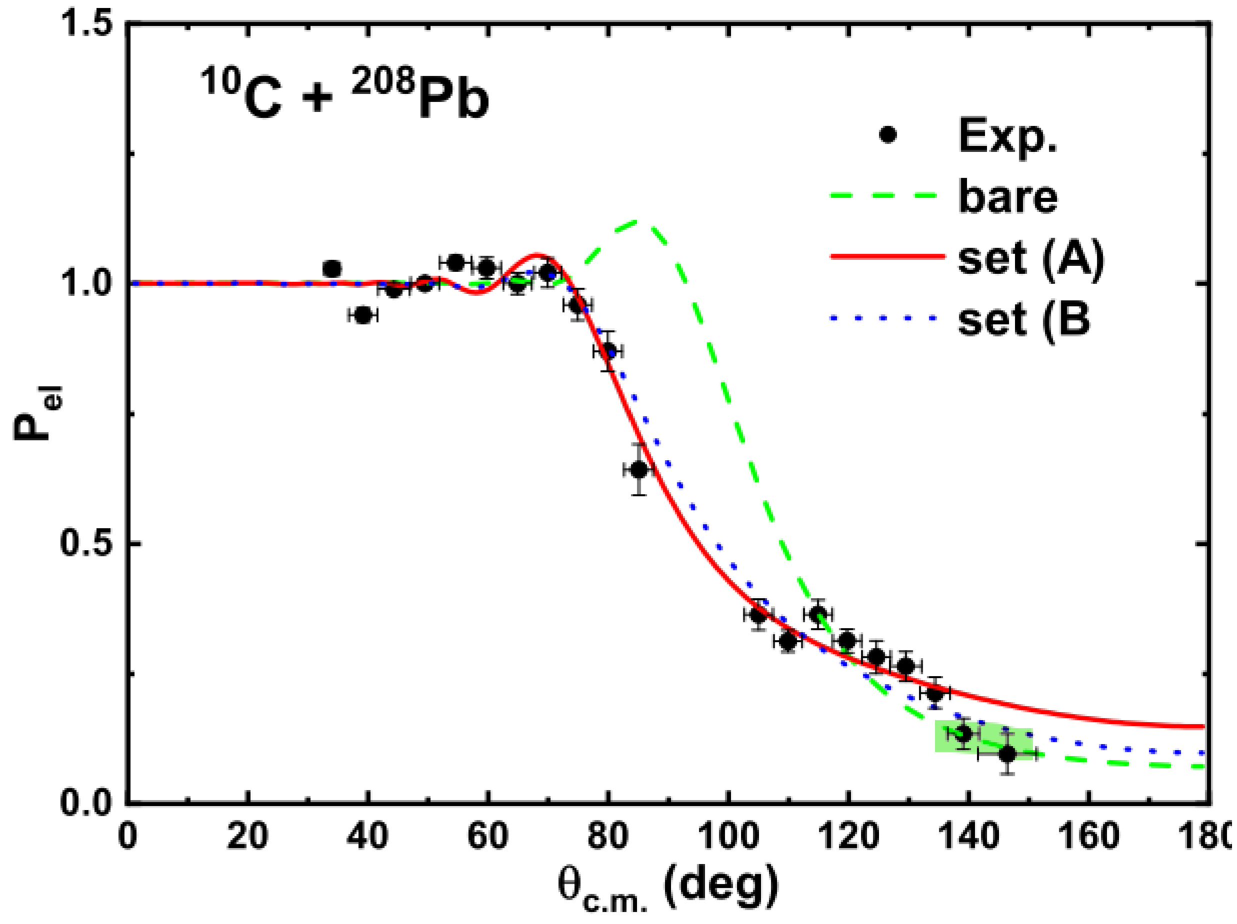

FIG. 4: $P_{\rm el}$ ratios for ^{10}C + ^{208}Pb system. Solid black circles denote the experimental data for ^{10}C + ^{208}Pb system at $E_{\rm lab}$ = 66.0 MeV. Solid red and dotted blue lines denote the theoretical ratios $P_{\rm el}$ using the parameter sets (A) and (B) in Table II, respectively. In contrast, dashed green line indicates $P_{\rm el}$ ratio only based on the bare potential in Eq. (2), which is identical to the dashed green line in Fig. 3 (b).

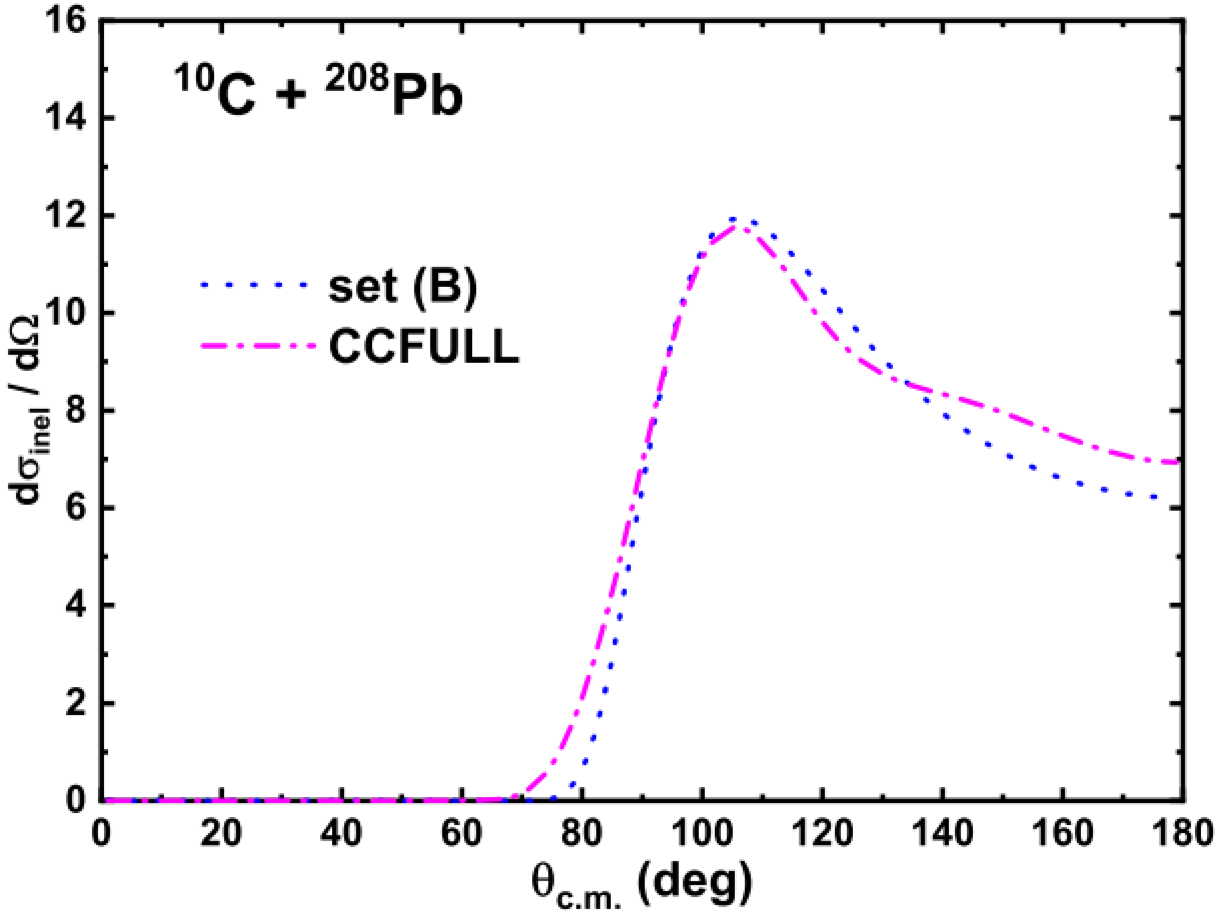

FIG. 5: Angular distribution of inelastic scattering cross-section for ^{10}C + ^{208}Pb system. Dash-dotted magenta line represent the theoretical angular distribution of inelastic scattering cross-section by the nuclear component obtained from CCFULL code [43]. In contrast, dotted blue line indicates the theoretical angular distribution of inelastic scattering cross-section obtained by fitting the dash-dotted magenta line based on parameter set (B) defined in Table II.

Today's Topic

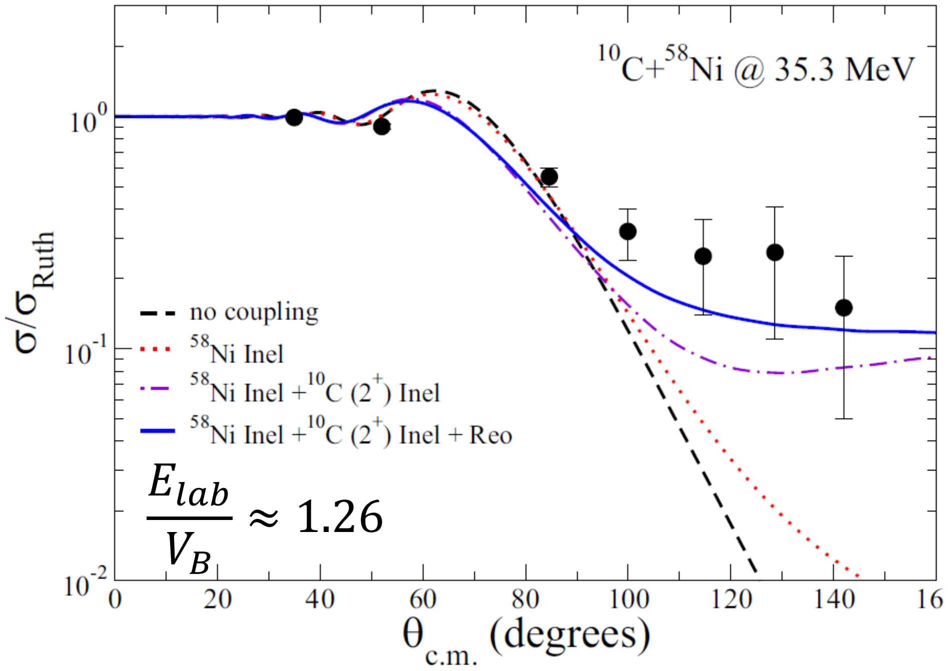

$^{10}C + ^{58}Ni$ @ 35.3MeV

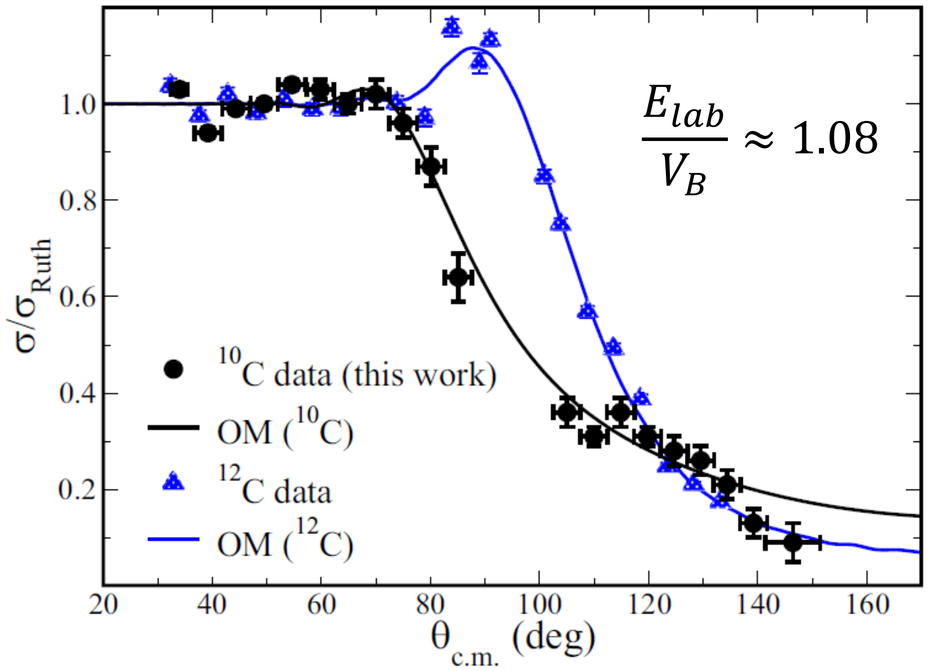

$^{10}C + ^{208}Pb$ @ 66MeV

$^{12}C + ^{208}Pb$ @ 64.9MeV

$^{10}C + ^{58}Ni$: PHYSICAL REVIEW C **100**, 034603 (2019) V. Guimarães *et al.*

$^{10}C + ^{208}Pb$: PHYSICAL REVIEW C **103**, 044613 (2021) R.Linares *et al.*

Submitted to PRC (2022)

1. Motivation
1-1. Exotic Light Nuclei
1-2. Low Energy Nuclear Reactions (LENR) for Exotic Nuclei

2. LENR for Carbon isotopes
2-1. Quasi-elastic scattering of C isotopes — Submitted to PRC (2022)
2-2. 12C + 12C scattering — PRC 104, 034306 (2021)

Dineutron?

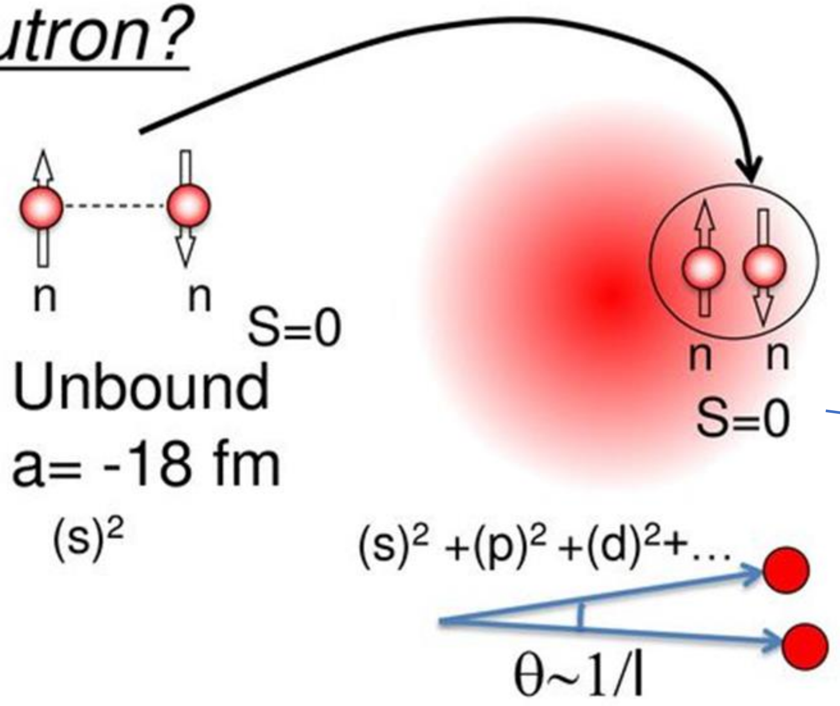

A.B.Migdal
Strongly correlated "**dineutron**"
on the **surface** of a nucleus
Sov.J.Nucl.Phys.238(1973).

Dineutron:
@ Low-dense neutron skin/halo?
/surface of neutron star?

M.Matsuo
PRC73,044309(2006),
A.Gezerlis, J.Carlson,
PRC81,025803(2010)

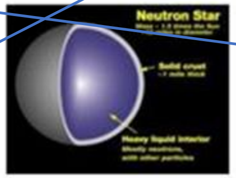

n-star

PHYSICAL REVIEW C **72**, 044321 (2005)

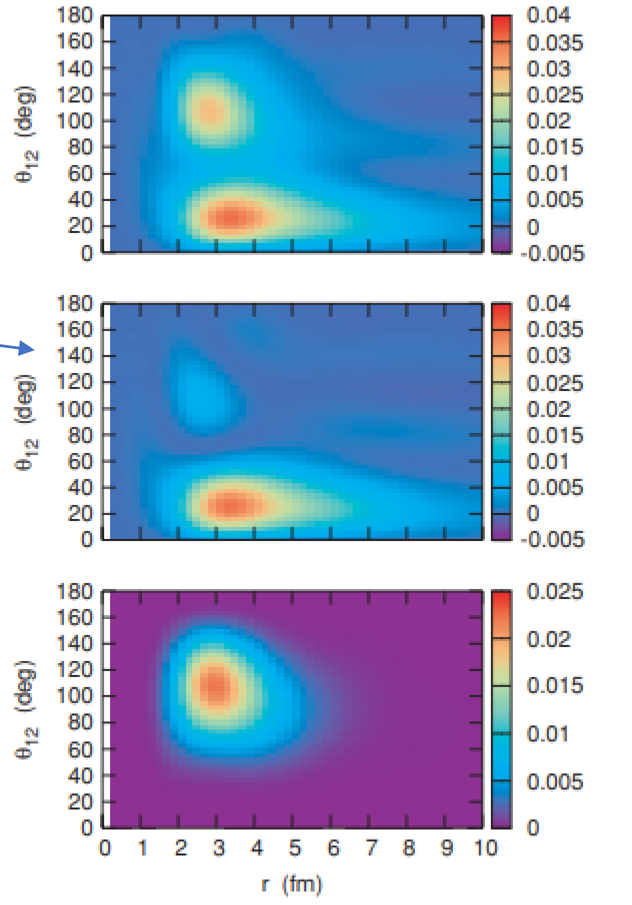

FIG. 2. (Color online) Same as Fig. 1, but for ^{11}Li.

Possible dineutron site:

2n Halo Nuclei?

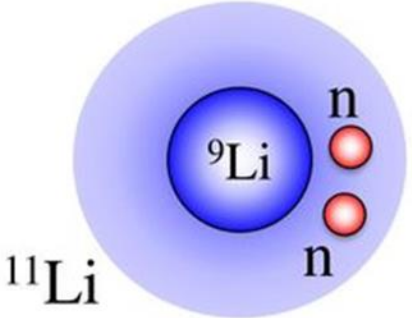

S_{2n}=0.37MeV

2n barely-unbound nuclei?

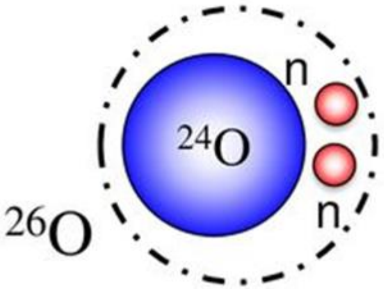

S_{2n}= –0.018(5) MeV
Kondo et al., PRL2016

Courtesy of J. Lee

Two-Nucleon Knockout Model

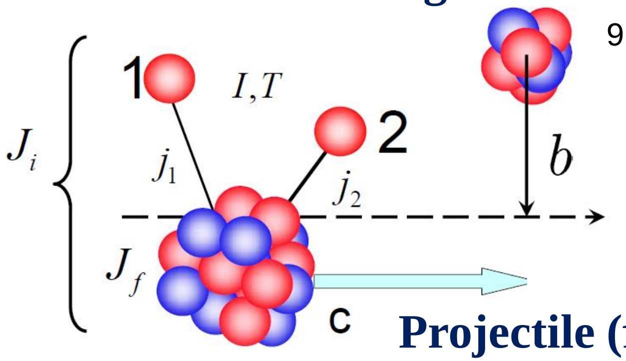

Theoretical Cross sections:

Reaction: Eikonal & Sudden approximation

Structure: 2*N* Overlap from Shell Model

J. Tostevin, B.A. Brown, PRC **74**, 064604 (2006)

E.C. Simpson and J. Tostevin et al., PRL **102**, 132502 (2009)

- 2n knockout from ^{34}Ar, ^{30}S, ^{26}Si

K. Yoneda et al., Phys. Rev. C 74 , 021303(R) (2006)

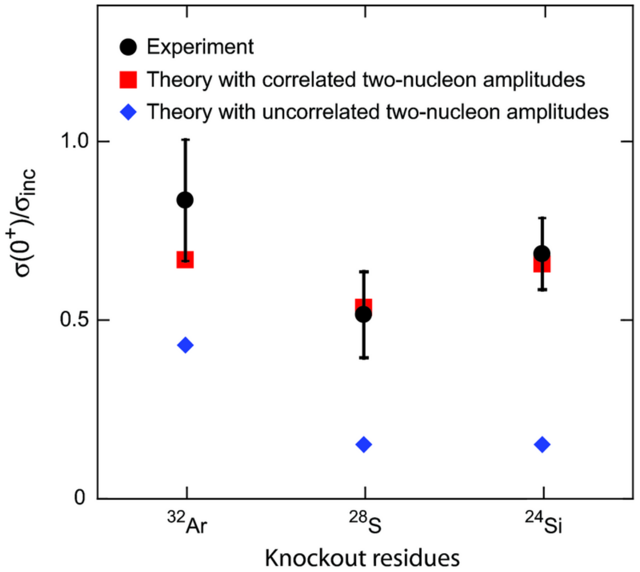

2*n* or 2*p* knockout (T=1)

D. Bazin et al., Phys. Rev. Lett. 91, 012501 (2003)
A. Gade et al., Phys. Rev. C 74 , 021302(R) (2006)
P. Fallon et al., PRC 81, 041302(R) (2010)

2N knockout cross sections
→ carry information of 2N correlations

Framework to quantitatively assess descriptions of *2n & 2p* T=1 correlations

Courtesy of J. Lee

PHYSICAL REVIEW C VOLUME 37, NUMBER 6 JUNE 1988

Fragmentation of carbon ions at 250 MeV/nucleon

J. M. Kidd
Naval Research Laboratory, Washington, D.C. 20375

P. J. Lindstrom
Lawrence Berkeley Laboratory, Berkeley, California 94720

H. J. Crawford
University of California, Berkeley, California 94720

G. Woods
Naval Research Laboratory, Orlando, Florida 32856

(Received 8 May 1987)

The single particle inclusive reactions $^{12}C + {}^{12}C \rightarrow x + \text{anything}$ $(3 \le Z \le 6)$ have been studied at 250 MeV/nucleon at nine production angles from 0° to 4°. Production cross sections for most isotopes $(Z > 2)$ were determined. The longitudinal and transverse momentum distributions were constructed. The results at this energy are compared to the data at other energies and to the model of Friedman. It appears that, after the Coulomb effects are separated, there is very little en dence in the fragmentation process.

1. Use the carbon beam from fragmentation by HIC and scatter off Carbon target.

2. Measure light ion and collect A=10 nuclei.

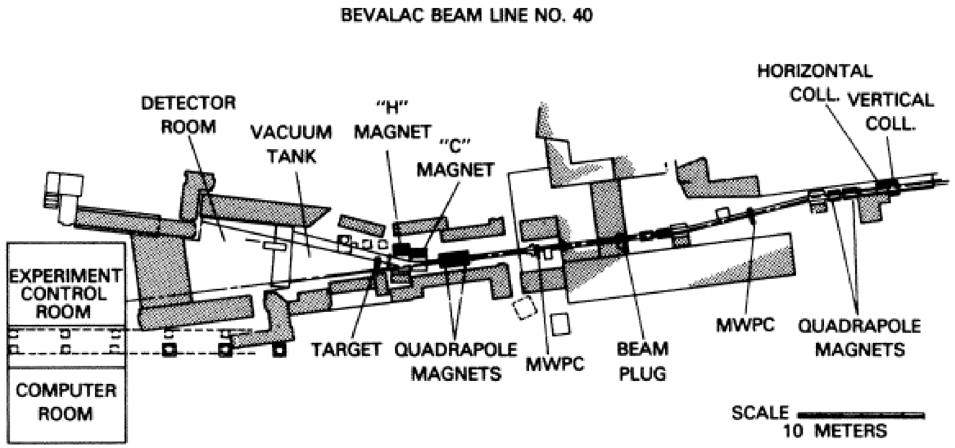

FIG. 1. Bevalac beam line 40.

TABLE VI. Carbon-data cross sections.

	(mb) 250 MeV/nucleon	1.05 GeV/nucleon[a]	2.1 GeV/nucleon[a]	Friedman[b]
^{6}Li	26.35±2.1	27.10±2.20	30.00±2.40	19.6
^{7}Li	>17.19±1.3	21.50±1.10	21.50±1.10	14.2
^{8}Li	>1.33±0.34	2.40±0.18	2.19±0.15	2.5
^{7}Be	22.64±1.49	18.60±0.90	18.40±0.90	13.3
^{9}Be	10.44±0.85	10.70±0.50	10.60±0.50	13.8
^{10}Be	5.88±9.70	5.30±0.30	5.81±0.29	7.1
^{11}Be	0.36±0.26			
^{8}B	<3.21±0.59	1.43±0.10	1.72±0.13	2.1
^{10}B	47.50±2.42	27.90±2.20	35.10±3.40	22.1
^{11}B	65.61±2.55	48.60±2.40	53.80±2.70	42.2
^{12}B	<0.49±0.67	0.10±0.01	0.10±0.01	
^{10}C	5.33±0.81	4.44±0.24	4.11±0.22	6.1
^{11}C	55.97±4.06	44.70±2.80	46.50±2.30	41.3

[a]Reference 4.
[b]Reference 10.

^{12}C – Interesting Physics Found & Hidden

Advanced Model *np* removal with T=0

First Calculations : np removal from ^{12}C (with Shell Model Calc. from B.A. Brown)

E.C. Simpson and J.A. Tostevin, PRC 83, 014605 (2011).

Residue	J_f^π	T	σ_{str}	σ_{ds}	σ_{dif}	σ_{-2N}
^{10}C	0+	1	1.59	0.64	0.06	2.30
	2+	1	1.96	0.71	0.06	2.74
-2n					Sum	5.04
					Expt.	4.11 ± 0.22
^{10}Be	0+	1	1.65	0.68	0.07	2.40
	2+	1	2.02	0.74	0.07	2.83
-2p	2+	1	0.88	0.32	0.03	1.23
	0+	1	0.04	0.01	0.00	0.06
					Sum	6.52
					Expt.	5.81 ± 0.29
^{10}B	3+	0	5.11	2.00	0.20	7.30
	1+	0	2.47	1.01	0.10	3.58
	0+	1	1.62	0.66	0.07	2.35
-np	1+	0	1.81	0.69	0.07	2.57
	2+	0	0.63	0.24	0.02	0.89
	3+a	0	1.14	0.43	0.04	1.62
	2+b	1	1.99	0.72	0.07	2.33
	1+a	0	0.30	0.10	0.01	0.41
	2+a	0	0.75	0.28	0.03	1.05
					Sum	19.02
					Expt.	35.10 ± 3.40

p-shell

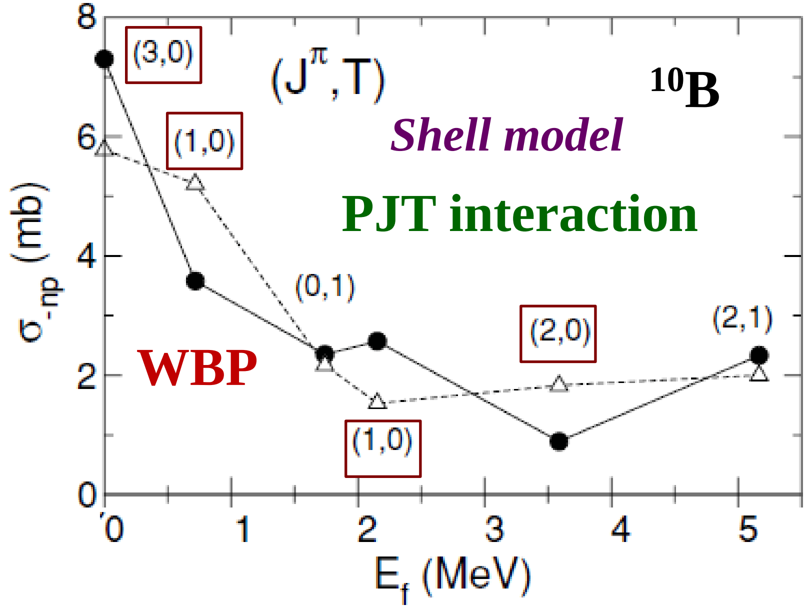

T=0 *np*-spatial correlations in the wave functions are insufficient

T = 0 cross-sections – sensitive to different effective interactions !

Courtesy of J. Lee

np-Correlations & 3-body Force

Structure Model → Eikonal-Theory Reaction Model → σ(theo)

✓ **Conventional Shell Model**
B.A. Brown (MSU)

✓ **No-core Shell Model (NCSM)**
(realistic 2-body and 3-body forces)
P. Navratil (TRIUMF)

⬇

Significant Increase in the T=0 Cross Sections !

T=0 cross section Sensitive to 3*N*-force !

***np*-removal of ^{12}C on ^{12}C target**

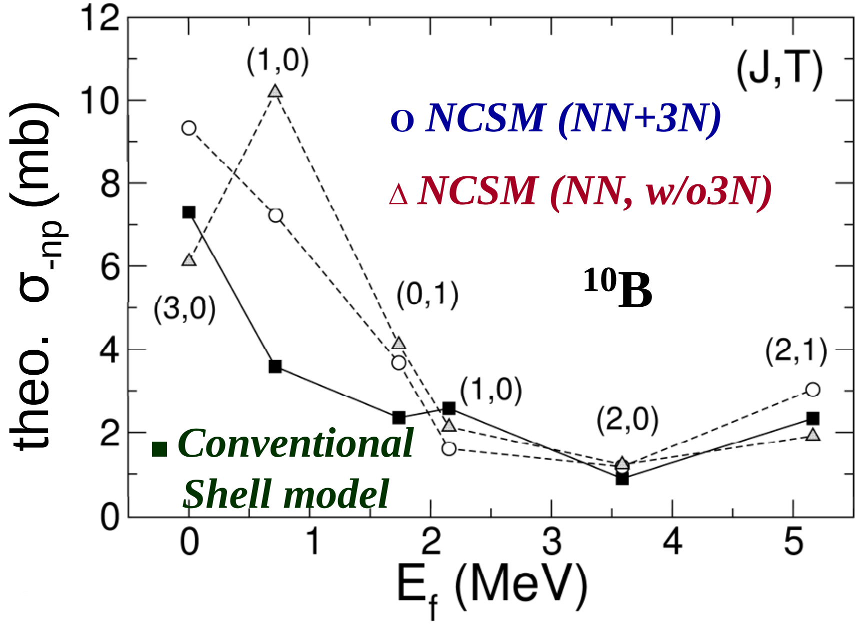

E. C. Simpson, P. Navrátil, R. Roth, and J. A. Tostevin
Phys. Rev. C **86**, 054609

- **TOSM** (tensor-optimized shell model) T. Myo (Osaka Tech)

Final-State-Exclusive Data needed to pin-point the physics !

Courtesy of J. Lee

TABLE III. Theoretical and experimental cross sections for two-nucleon knockout from ^{12}C, for projectile energies of 250, 1050, an 2100 MeV per nucleon. All cross sections are in mb. The TNAs used were calculated using the WBP interaction.

Energy	^{10}Be			^{10}C			^{10}B		
MeV/u	$\sigma_{\rm th}$	$\sigma_{\rm exp}$	$\sigma_{\rm exp}/\sigma_{\rm th}$	$\sigma_{\rm th}$	$\sigma_{\rm exp}$	$\sigma_{\rm exp}/\sigma_{\rm th}$	$\sigma_{\rm th}$	$\sigma_{\rm exp}$	$\sigma_{\rm exp}/\sigma_{\rm th}$
250 [12]	7.48	5.88 ± 9.70	0.79 ± 1.30	5.80	5.33 ± 0.81	0.92 ± 0.14	21.57	47.50 ± 2.42	2.20 ± 0.1
1050 [13]	6.62	5.30 ± 0.30	0.80 ± 0.05	5.13	4.44 ± 0.24	0.87 ± 0.05	19.27	27.90 ± 2.20	1.45 ± 0.1
2100 [13]	6.52	5.81 ± 0.29	0.89 ± 0.04	5.04	4.11 ± 0.22	0.82 ± 0.04	19.02	35.10 ± 3.40	1.84 ± 0.1

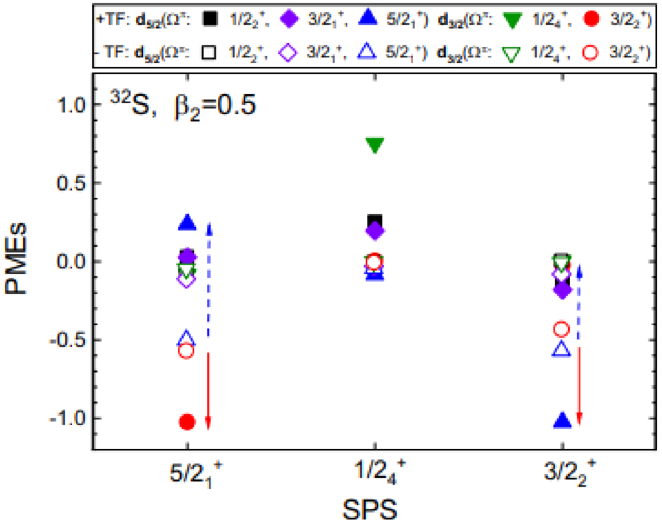

FIG. 4. The TF effects on pairing matrix elements (PMEs) by the G matrix, $G(aacc, J = 1, T = 0)$ in Eq. (4), as a function of the single-particle state (SPS) in the Nilsson basis with and without the TF for ^{32}S at $\beta_2 = 0.5$. The solid (empty) symbols denote the results with (without) the TF. The configurations written below the abscissa correspond to a, while those in the small box are c configurations in the G matrix.

TABLE III. Ratios of the np knockout to nn and pp knockout cross sections for ^{12}C + ^{12}C reactions. Calculated results are given in the la four columns in different deformations with and without the TF (denoted as with TF and without TF) by using the number of pairs in Fig. 1(calculated by Eq. (11). Experimental data are taken from Ref. [47].

Ratio	Energy	Exp. data	Without TF $\beta_2 = 0.3$	With TF $\beta_2 = 0.3$	Without TF $\beta_2 = 0.5$	With TF $\beta_2 = 0.5$
$\sigma_{-np}/\sigma_{-nn}$	250 MeV	47.50/5.33 = 8.91				
	1.05 GeV	27.90/4.44 = 6.28	7.8	4.5	4.0	9.7
	2.1 GeV	35.10/4.11 = 8.54				
$\sigma_{-np}/\sigma_{-pp}$	250 MeV	47.50/5.88 = 8.09				
	1.05 GeV	27.90/5.30 = 5.26	7.8	4.5	4.0	9.7
	2.10 GeV	35.10/5.81 = 6.04				

1. Motivation
1-1. Exotic Light Nuclei
1-2. Low Energy Nuclear Reactions (LENR) for Exotic Nuclei

2. LENR for Carbon isotopes
2-1. Quasi-elastic scattering of C isotopes — Submitted to PRC (2022)
2-2. 12C + 12C scattering — PRC 104, 034306 (2021)

3. LENR for 10Be
3-1. Cosmological Origin of 10Be — ArXiv: 2203.13365: ApJS, in press, (2022)

Introduction - meteorite data

- 논문에 있는 운석 데이터를 비교

Nature Communications, (2016), 7

nature COMMUNICATIONS

ARTICLE

Received 14 Jan 2016 | Accepted 20 Oct 2016 | Published 22 Nov 2016 DOI: 10.1038/ncomms13639 OPEN

Evidence from stable isotopes and ^{10}Be for solar system formation triggered by a low-mass supernova

Projjwal Banerjee[1], Yong-Zhong Qian[1], Alexander Heger[2,3] & W.C. Haxton[4]

About 4.6 billion years ago, some event disturbed a cloud of gas and dust, triggering the gravitational collapse that led to the formation of the solar system. A core-collapse supernova, whose shock wave is capable of compressing such a cloud, is an obvious candidate for the initiating event. This hypothesis can be tested because supernovae also produce telltale patterns of short-lived radionuclides, which would be preserved today as isotopic anomalies. Previous studies of the forensic evidence have been inconclusive, finding a pattern of isotopes differing from that produced in conventional supernova models. Here we argue that these difficulties either do not arise or are mitigated if the initiating supernova was a special type, low in mass and explosion energy. Key to our conclusion is the demonstration that short-lived ^{10}Be can be readily synthesized in such supernovae by neutrino interactions, while anomalies in stable isotopes are suppressed.

10Be can produced from the SN !

Introduction - meteorite data

- 논문에 있는 운석 데이터를 비교

Nature Communications, (2016), 7

Meteorite

Table 1 | Yields of short-lived radionuclides from an 11.8-solar-mass core-collapse supernova.

R/I	τ_R (Myr)	Y_R ($M_\odot$)	$X_I^\odot$	$(N_R/N_I)_{ESS}$ Data	Case 1	Case 2	Case 3
$^{10}Be/^{9}Be$	2.00	3.26(−10)	1.40(−10)	(7.5±2.5)(−4)	6.35(−4)	6.35(−4)	5.20(−4)
$^{26}Al/^{27}Al$	1.03	2.91(−6)	5.65(−5)	(5.23±0.13)(−5)	1.02(−5)	9.90(−6)	5.77(−6)
$^{36}Cl/^{35}Cl$	0.434	1.44(−7)	3.50(−6)	~(3-20)(−6)	2.00(−6)	1.45(−6)	6.15(−7)
$^{41}Ca/^{40}Ca$	0.147	3.66(−7)	5.88(−5)	(4.1±2.0)(−9)	3.40(−9)	2.74(−9)	2.26(−9)
$^{53}Mn/^{55}Mn$	5.40	1.22(−5)	1.29(−5)	(6.28±0.66)(−6)	4.04(−4)	6.39(−6)	6.16(−6)
$^{60}Fe/^{56}Fe$	3.78	3.08(−6)	1.12(−3)	~1(−8);(5-10)(−7)	9.80(−7)	9.80(−7)	1.10(−7)
$^{107}Pd/^{108}Pd$	9.38	1.37(−10)	9.92(−10)	(5.9±2.2)(−5)	6.27(−5)	6.27(−5)	5.72(−5)
$^{135}Cs/^{133}Cs$	3.32	2.56(−10)	1.24(−9)	~5(−4)	7.51(−5)	7.51(−5)	3.18(−5)
$^{182}Hf/^{180}Hf$	12.84	4.04(−11)	2.52(−10)	(9.72±0.44)(−5)	7.36(−5)	7.36(−5)	6.34(−6)
		8.84(−12)			1.60(−5)	1.60(−5)	2.37(−6)
$^{205}Pb/^{204}Pb$	24.96	9.20(−11)	3.47(−10)	~1(−4);1(−3)	1.27(−4)	1.27(−4)	7.78(−5)

Comparisons are made to the corresponding isotopic ratios deduced from meteoritic data. Case 1 estimates are calculated from equation (1) using the approximate best-fit f and Δ of Fig. 2, assuming no fallback. The higher and lower yields for ^{182}Hf are obtained from the laboratory and estimated stellar decay rates[47] of ^{181}Hf, respectively. Case 2 (3) is a fallback scenario in which only 1.5% of the innermost 1.02×10^{-2} solar mass (0.116 solar mass) of shocked material is ejected. With guidance from refs 22,31, well-determined data are quoted with 2σ errors, while data with large uncertainties are preceded by '~'. Note that $x(-y)$ denotes $x \times 10^{-y}$. Data references are: ^{10}Be (refs 14,16,18,19), ^{26}Al (refs 2,32), ^{36}Cl (refs 33-35), ^{41}Ca (refs 36,37), ^{53}Mn (ref. 38), ^{60}Fe (refs 39,40), ^{107}Pd (ref. 41), ^{135}Cs (ref. 42), ^{182}Hf (ref. 43) and ^{205}Pb (refs 44,45).

13. Cyburt, R. H. *et al.* The JINA REACLIB database: its recent updates and impact on type-I X-ray bursts. *Astrophys. J. Suppl. Ser.* **189,** 240–252 (2010).

particles (SEPs[10,11]) associated with activities of the proto-Sun. It was noted in Yoshida *et al.*[12] that ^{10}Be can be produced by neutrino interactions in CCSNe, but the result was presented for a single model and no connection to meteoritic data was made. Further, that work adopted an old rate for the destruction reaction $^{10}Be(\alpha,n)^{13}C$ that is orders of magnitude larger than currently recommended[13], and therefore, greatly underestimated the ^{10}Be yield.

^{10}Be has been observed in the form of a ^{10}B excess in a range of meteoritic samples. Significant variations across the samples

Moreover the data of the ratio 10Be/9Be was obtained from the meteorite analysis.
Note that 10Be is unstable and 9Be is stable.
But previous calculation predicted that 10Be cannot be produced by the neutrino-process because the destruction channel 10Be(a,n)13C was overestimated i.e. 10Be was destructed fully.

Introduction

- Short-lived Radioactive Nuclei

Progress in Particle and Nuclear Physics, (2018), 1-47, 102

Table 3
List of stellar nucleosynthesis sites and the nucleosynthetic processes occurring within them that are responsible for the production of the SLRs and stable reference isotopes listed in Column 3. Column 4 indicates if the site of production is important in terms of GCE (**M**=Major) or not (*m*=minor); **M**/*m* indicates that it is still debated whether the site is major or minor. Indicative references are listed in Column 5.

Stellar site	Process	Products	Relevance	Ref.
Low-mass AGBs	*s* process	^{107}Pd, ^{108}Pd	**M**	[93,94]
		^{135}Cs, ^{133}Cs	**M**	
		^{182}Hf, ^{180}Hf	**M**	
		^{205}Pb, ^{204}Pb	**M**	
Massive and Super-AGBs	p captures	^{26}Al	*m*	[80,94–96]
	n captures	^{41}Ca, ^{36}Cl, ^{60}Fe	*m*	
	s process	^{107}Pd, ^{135}Cs, ^{182}Hf	*m*	
WR stars	p captures	^{26}Al	**M**	[97,98]
	n captures	^{41}Ca, ^{36}Cl	*m*	
	n captures	^{97}Tc, ^{107}Pd, ^{135}Cs, ^{205}Pb	*m*	
CCSNe	p captures+explosive	^{26}Al, ^{27}Al	**M**	[99]
	n captures	^{60}Fe	**M**	[99]
	n captures	^{36}Cl, ^{41}Ca	**M**	[94,100]
	C/Ne/O burning	^{35}Cl, ^{40}Ca	**M**	[101]
	NSE	^{53}Mn, ^{55}Mn, ^{56}Fe	**M**/*m*[a]	[101]
	n captures	^{107}Pd, ^{126}Sn, ^{135}Cs	*m*	[102]
		^{129}I, ^{182}Hf, ^{205}Pb	*m*	
	α-rich freezeout	^{92}Nb, ^{92}Mo, ^{97}Tc, ^{98}Tc	**M**/*m*	[103]
	γ process	^{144}Sm, ^{146}Sm	**M**/*m*	[103,104]
	ν process	$\boxed{^{10}\mathrm{Be}}$, ^{92}Nb	*m*	[105,106]
SNIa	NSE	^{53}Mn, ^{55}Mn, ^{56}Fe	**M**	[107]
	γ process	^{92}Nb, ^{93}Nb, ^{146}Sm, ^{144}Sm	**M**/*m*	[108]
		^{97}Tc, ^{98}Tc, ^{98}Ru	**M**/*m*	
NSMs/special CCSNe	*r* process	^{107}Pd, ^{108}Pd, ^{126}Sn, ^{124}Sn	**M**	[109][b]
		^{135}Cs, ^{133}Cs, ^{129}I, ^{127}I	**M**	
		^{182}Hf, ^{180}Hf	**M**	
		^{247}Cm, ^{235}U, ^{244}Pu, ^{238}U	**M**	[110,111]
novae	p captures	^{26}Al	*m*	[112]
CRs	non-thermal	^{7}Be, $\boxed{^{10}\mathrm{Be}}$, ^{9}Be	**M**	[32]
		^{26}Al, ^{41}Ca, ^{36}Cl, ^{53}Mn	*m*	[113]

[a] The current understanding is that roughly 1/3 of the abundances of the Fe-peak elements in the Galaxy are produced by CCSNe, with the rest coming from SNIa.
[b] Abundances to be derived using the *s*-process predictions provided in the reference via the *r*-residual method, where the *r*-process abundance is given by the Solar System abundance minus the *s*-process abundance.

[105] Nature Communications, (2016), 7

But, even if we use the correct rate for the (a,n) reaction,
the production rate is smaller than the production by the cosmic ray, which
is a kind of the spallation by cosmic rays.

That is the reason why the main mechanism is the spallation by the CR. Is it true?

Main nuclear reactions for the production of 10Be in the neutrino process

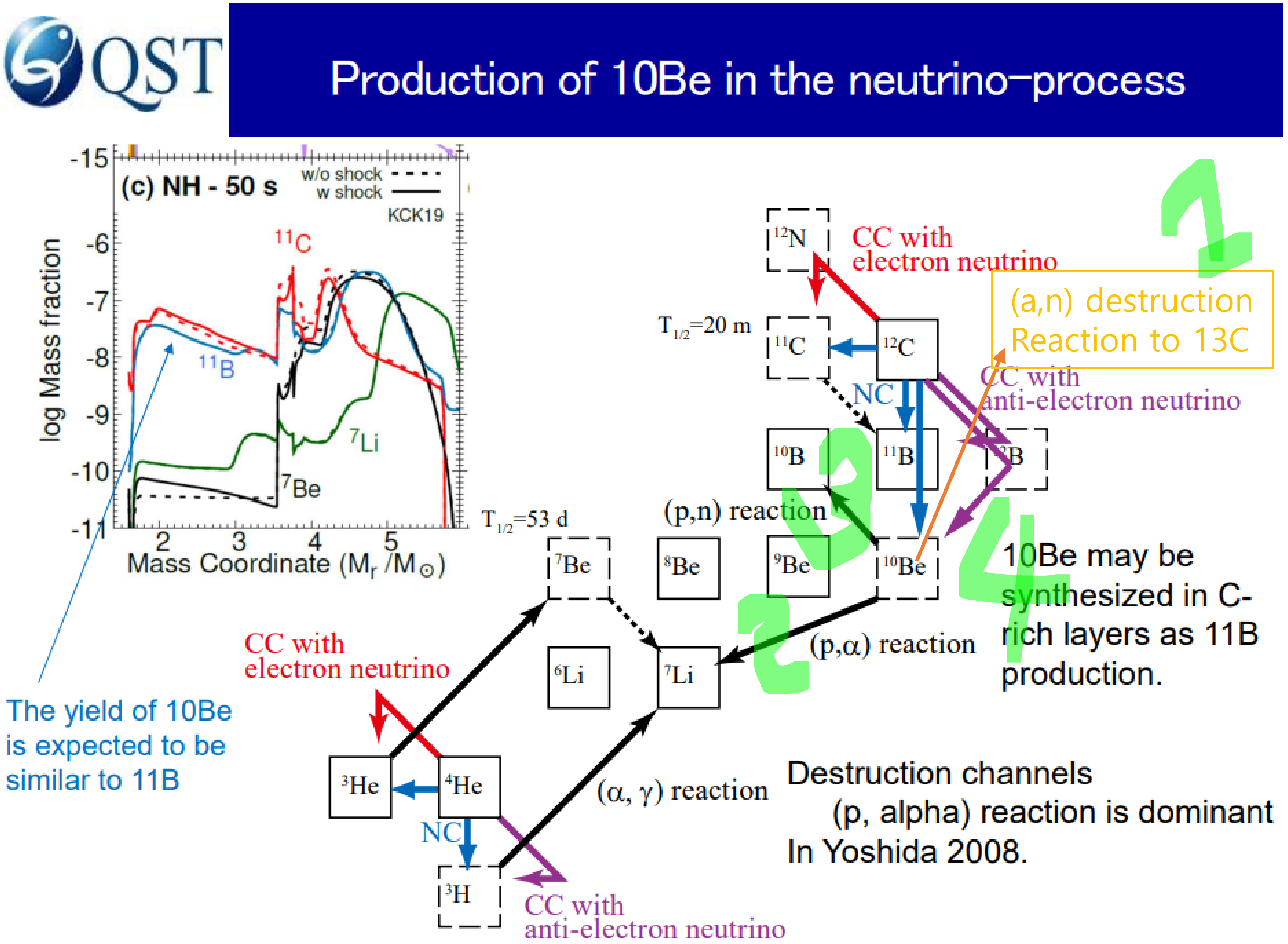

Destruction Reactions (a,n) and (p,a) are fixed by data and new calculations.
But the problem remained is the (p,n) reaction and its inverse reactions, because we do not have data and theoretical calculations are still questionable.

Mass Coordinate vs Mass Fraction

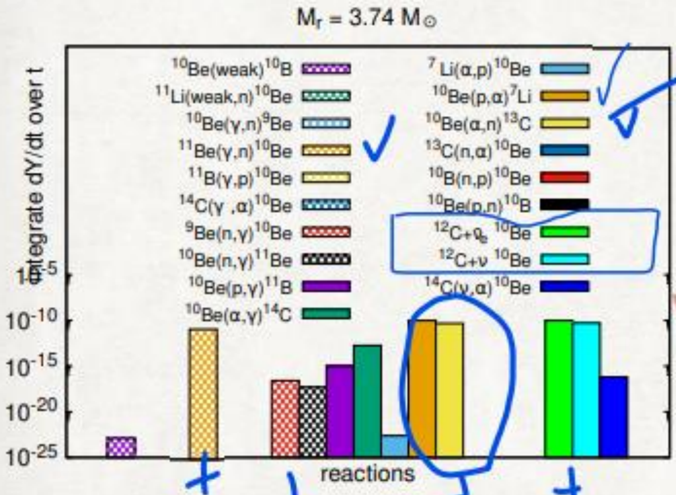

Not me

Main production

$$^{12}\mathrm{C} + \bar{\nu}_e \rightarrow {}^{10}\mathrm{Be}$$

Main destruction

$$^{10}\mathrm{Be}(p,\alpha)^{7}\mathrm{Li}$$

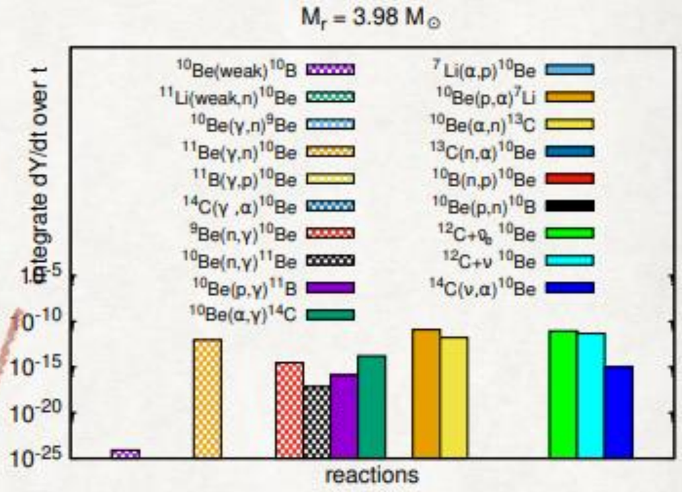

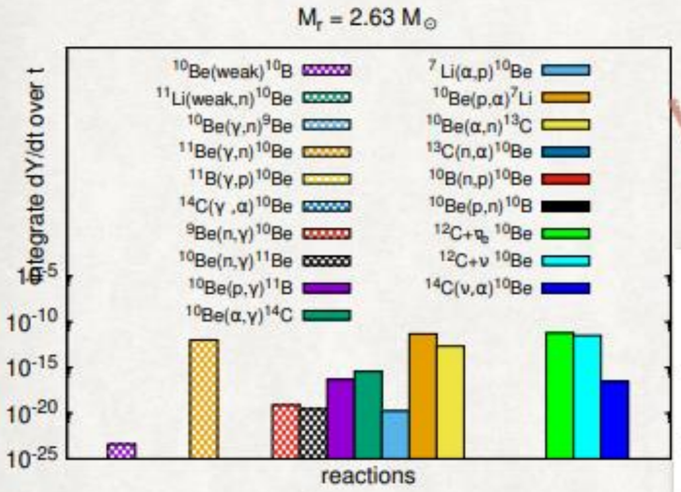

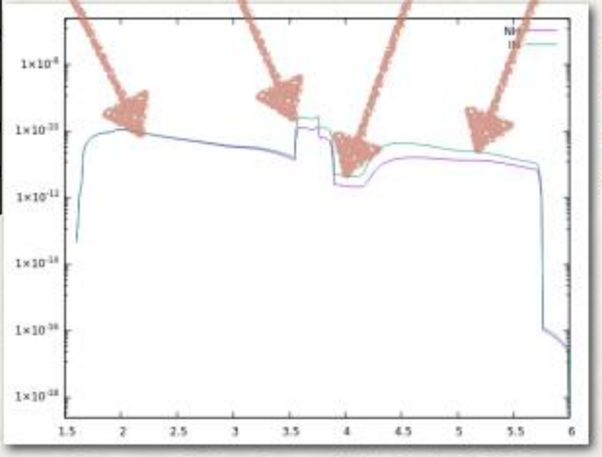

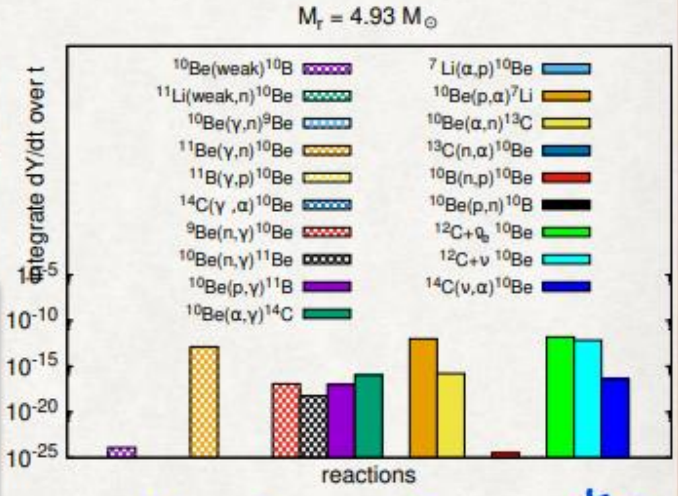

^{10}Be(p,n)^{10}B contr. is small, but very impor.

Histograms for NH case

이전 계산은 ^{10}Be이 O(-22) 정도로 작았음

(n,p) and (p,n) reactions by Talys which was used in the process

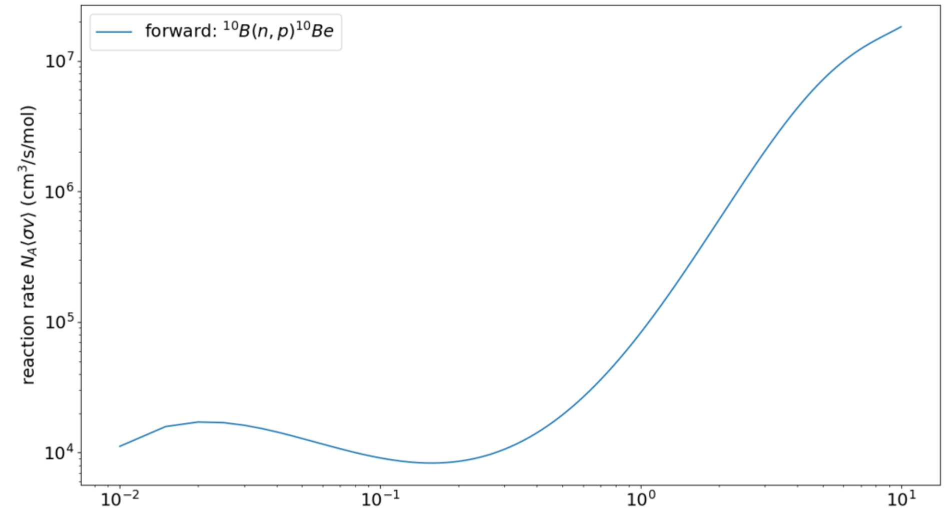

(0.01 T9 < T <10 T9)

0.00086 MeV (= 0.086 keV) < E < 0.86 MeV)

1MeV=1.16*10^10 Kelvin

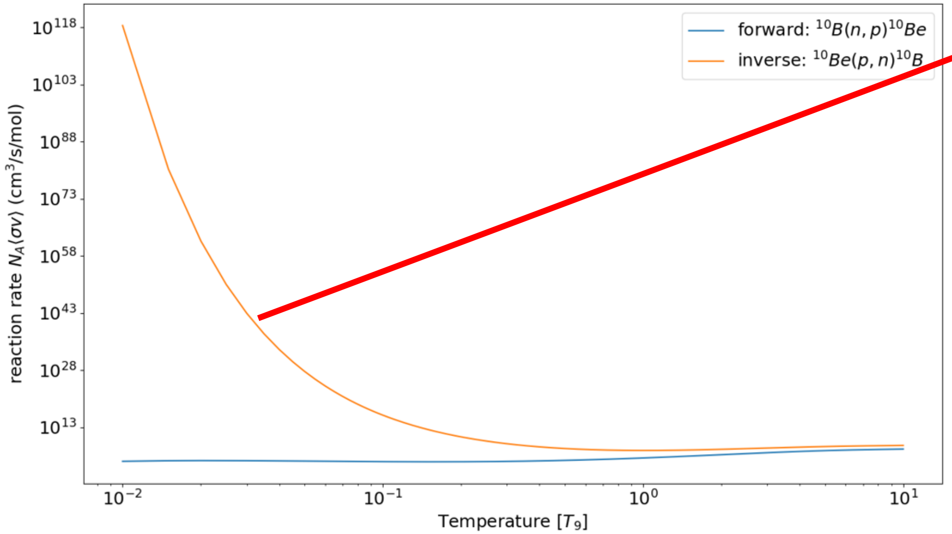

Destruction reaction 10Be(p,n)10B is too large.
It is calculated by Talys !

That is the reason 10Be was too small O(-22)
in the previous calculation which used the Talys results!!

(n,p) and (p,n) reactions

10B(n,p)10Be rection from JENDL-5

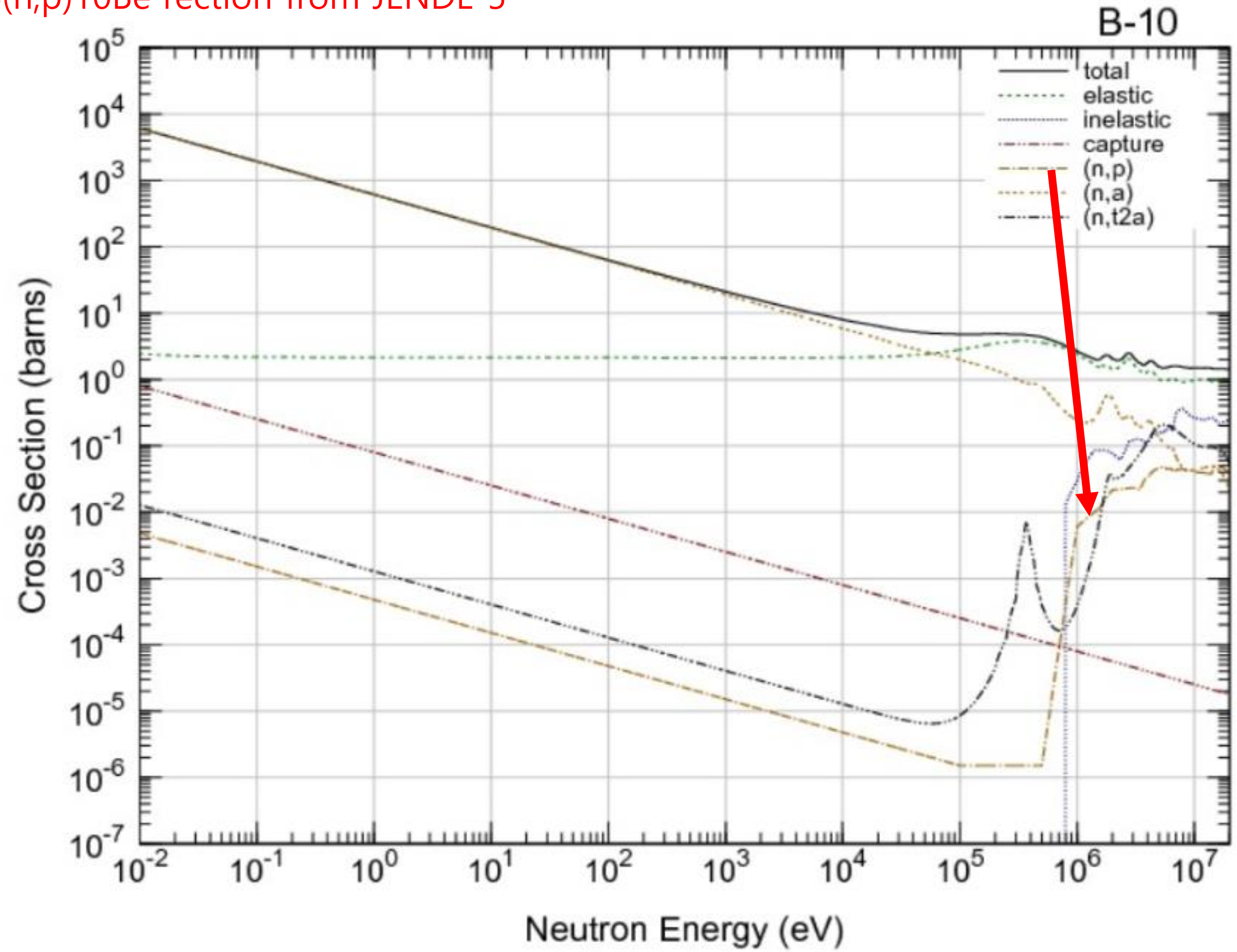

10Be(p,n)10B rection by Chiba using 10B(n,p)10Be reaction data from JENDL-5

(n,p) and (p,n) reactions

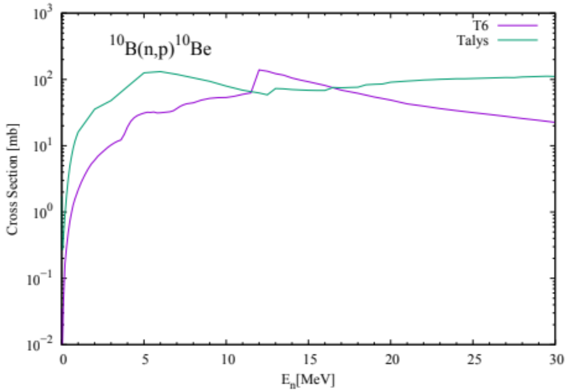

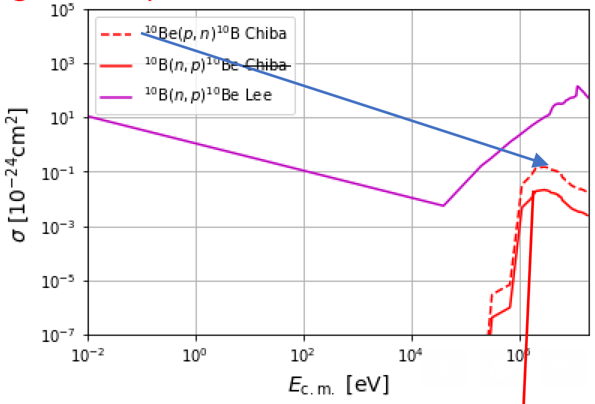

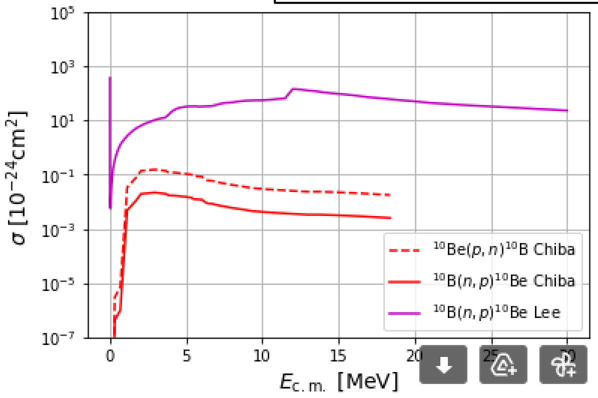

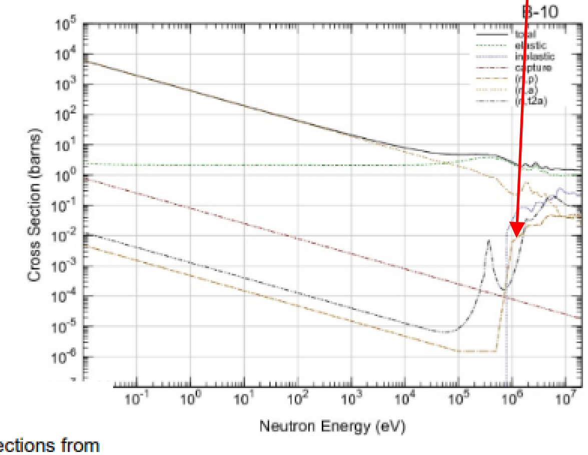

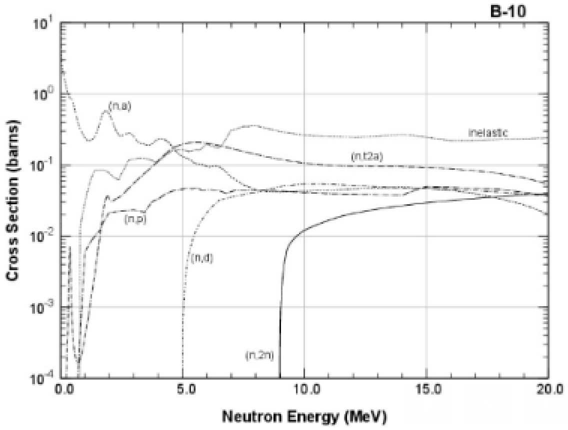

Dear Cheoun-san,

Chiba-san has calculated the 10Be(p,n)10B reaction cross sections from the well evaluated inverse reaction
10B(n,p)10Be in the JENDL-5 database.
The values in the energy region of E < 1MeV are lower than
0.01 mbarn. This suggests that 10Be destruction channel in supernova neutrino-process is much small.

Forward Reaction and inverse reaction

Cross section

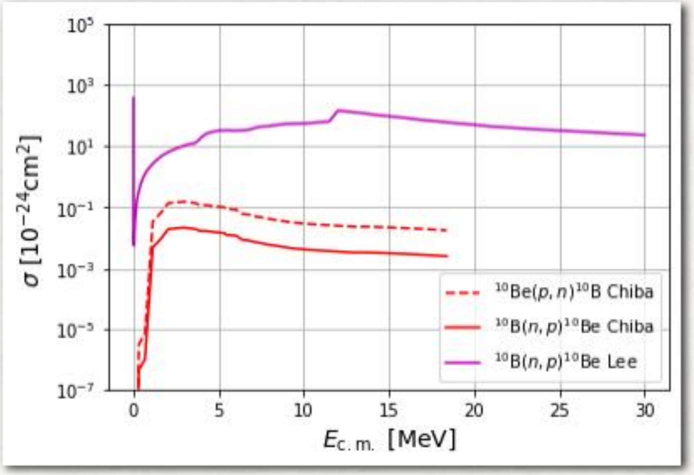

Thermonuclear reaction rate

The index "kusa" denotes TALYS-1.8 code (2015) in Kusakabe et al, APJ, (2019), 164, 872 (2)

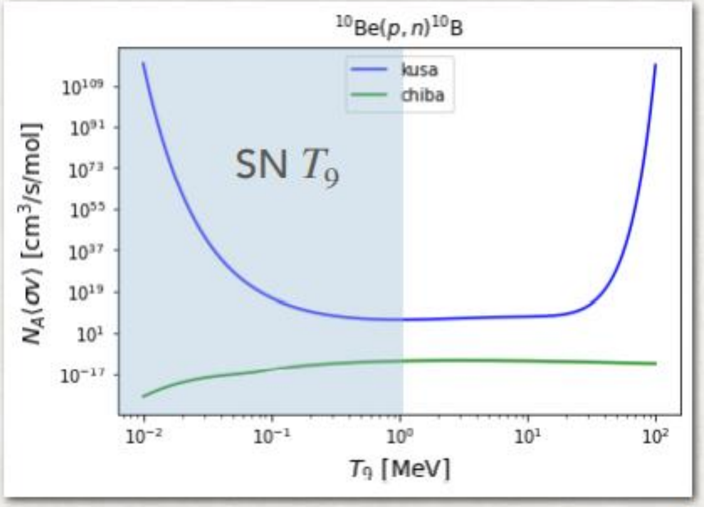

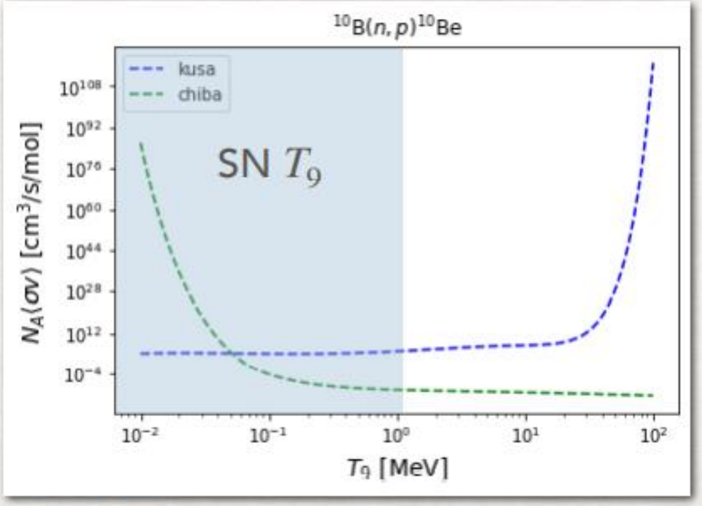

If we use the new data for the (n,p) and (p,n) reactions deduced from JENDL data,
The destruction becomes small, and the construction is larger than those by the Talys. **Be10 abundance is up !!**

Previous calculation

t~50s

		^{10}Be and ^{53}Mn				^{9}Be and ^{55}Mn
R/I	Mass hierarchy	Life time (Myr)	Mass yield **ONeMg**	Mass yield **He (+C/O)**	Mass yield	Solar abundance (Lodders et al. 2009)
^{10}Be/^{9}Be	NH	2.00	6.672E-26	2.444E-24	2.51072E-24	1.5088E-10
	IH	2.00	4.802E-21	2.170E-23	4.8237E-21	1.5088E-10
^{53}Mn/^{55}Mn	NH	5.40	5.383E-08	2.638E-09	5.6468E-08	1.3891E-05
	IH	5.40	5.303E-08	1.324E-09	5.4354E-08	1.3891E-05

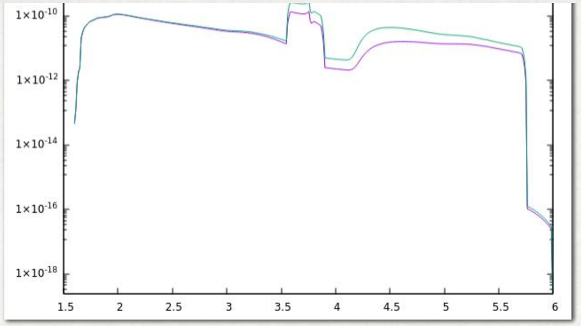

~~Group Meeting July 8th 2022~~

Current calculation

tegrated r

$$\left(\frac{N_{^{10}\mathrm{Be}}}{N_{^{9}\mathrm{Be}}}\right)_{ESS} \sim f \frac{(X_{^{10}\mathrm{Be}})_{SN}}{(X_{^{9}\mathrm{Be}})_{\odot} + (X_{^{9}\mathrm{Be}})_{SN}} \exp\left(\frac{-\Delta}{2\ \mathrm{Myr}}\right)$$

t~50s

$(M_{\odot})$	Be10	Be9	Be9 (solar mass fraction)
NH	1.572E-10	8.181E-11	1.51E-10
IH	2.185E-10	1.060E-10	1.51E-10

T. Hayakawa et al. Astrophysical Journal Letters, 779, (2013)

Nature Communications, (2016), 7

1) $f \sim 1 \times 10^{-4}$ and $\Delta \sim 1$ Myr

2) $f \sim 3 \times 10^{-3}$ and $\Delta \sim 1$ Myr

3) $f \sim 5 \times 10^{-4}$ and $\Delta \sim 1$ Myr

Table 1 | Yields of short-lived radionuclides from an 11.8-solar-mass core-collapse supernova.

R/I	**τ_R (Myr)**	**Y_R ($M_{\odot}$)**	**$X_I^{\odot}$**	**$(N_R/N_I)_{ESS}$**			
				Data	**Case 1**	**Case 2**	**Case 3**
^{10}Be/^{9}Be	2.00	3.26(−10)	1.40(−10)	$\boxed{(7.5 \pm 2.5)(-4)}$	6.35(−4)	6.35(−4)	5.20(−4)

$$(7.5 \pm 2.5) \times 10^{-4} \sim f \frac{(X_{^{10}\mathrm{Be}})_{SN}}{(X_{^{9}\mathrm{Be}})_{\odot} + (X_{^{9}\mathrm{Be}})_{SN}} \exp\left(\frac{-\Delta}{2\ \mathrm{Myr}}\right)$$

Parameter set	1)	2)	3)	meteorite
NH	4.551E-05	1.365E-03	2.275E-04	[illegible]
IH	5.730E-05	1.719E-03	2.865E-04	

Summary 1
As suggested by Nature, we used new data for 10Be(a,n)13C from JINA REACLIB .
But 10Be abundance is very small.

Summary 2
Previous calculation used the Talys results for 10Be(p,n)10B, which destroyed 10Be.
But new calculations based on JENDL-5 showed that the (p,n) reaction is small,
so that
10Be abundance increases.

The CEX is really important and needs the experimental data !!

Production of 10Be in the neutrino-process

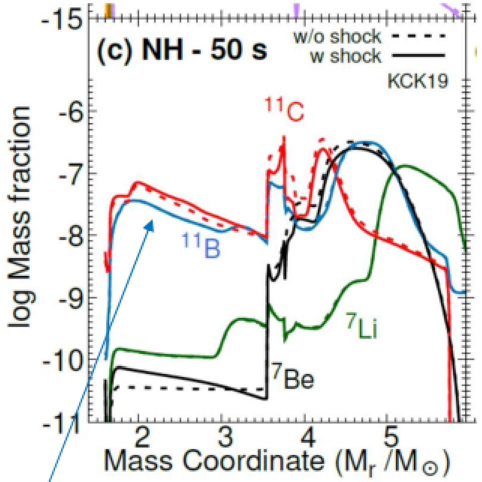

The yield of 10Be is expected to be similar to 11B

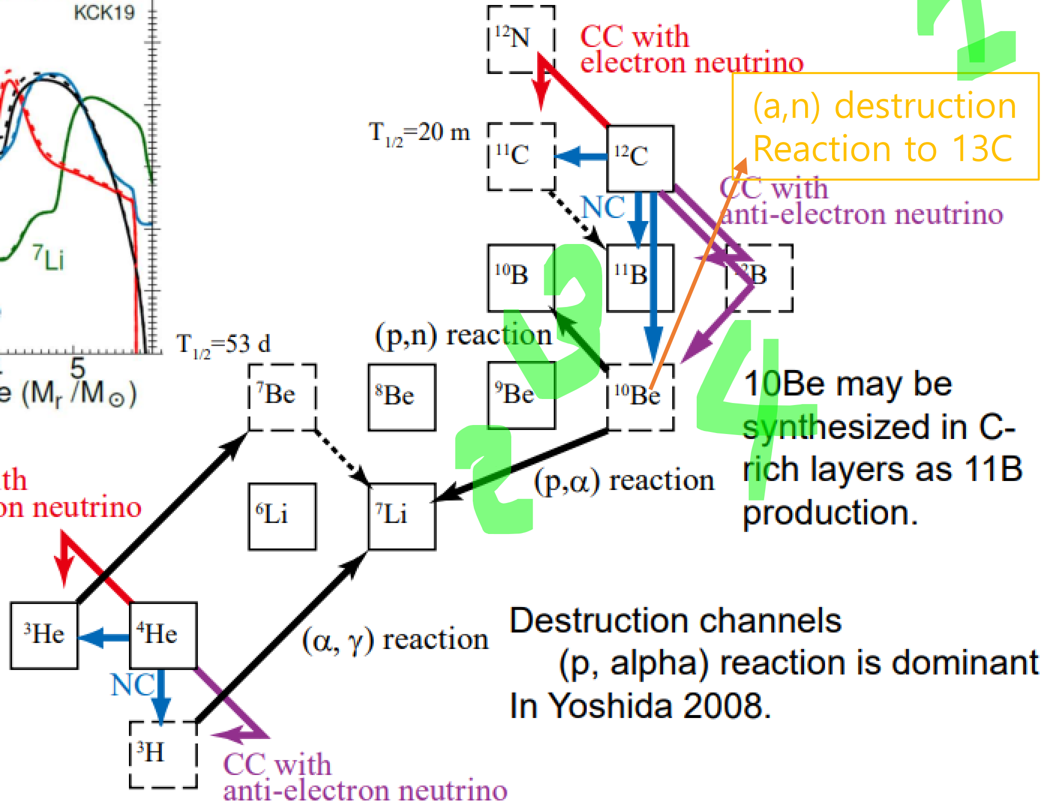

10Be may be synthesized in C-rich layers as 11B production.

Destruction channels
(p, alpha) reaction is dominant
In Yoshida 2008.

However, there is another production channel from 11Be, 11Be(g,n)10Be.

Why $^{11}\mathrm{Be}(\gamma, n)^{10}\mathrm{Be}$ is so high?

^{11}Be은 주로 $^{12}\mathrm{C}+\bar{\nu}_e$로 부터 생기긴 함

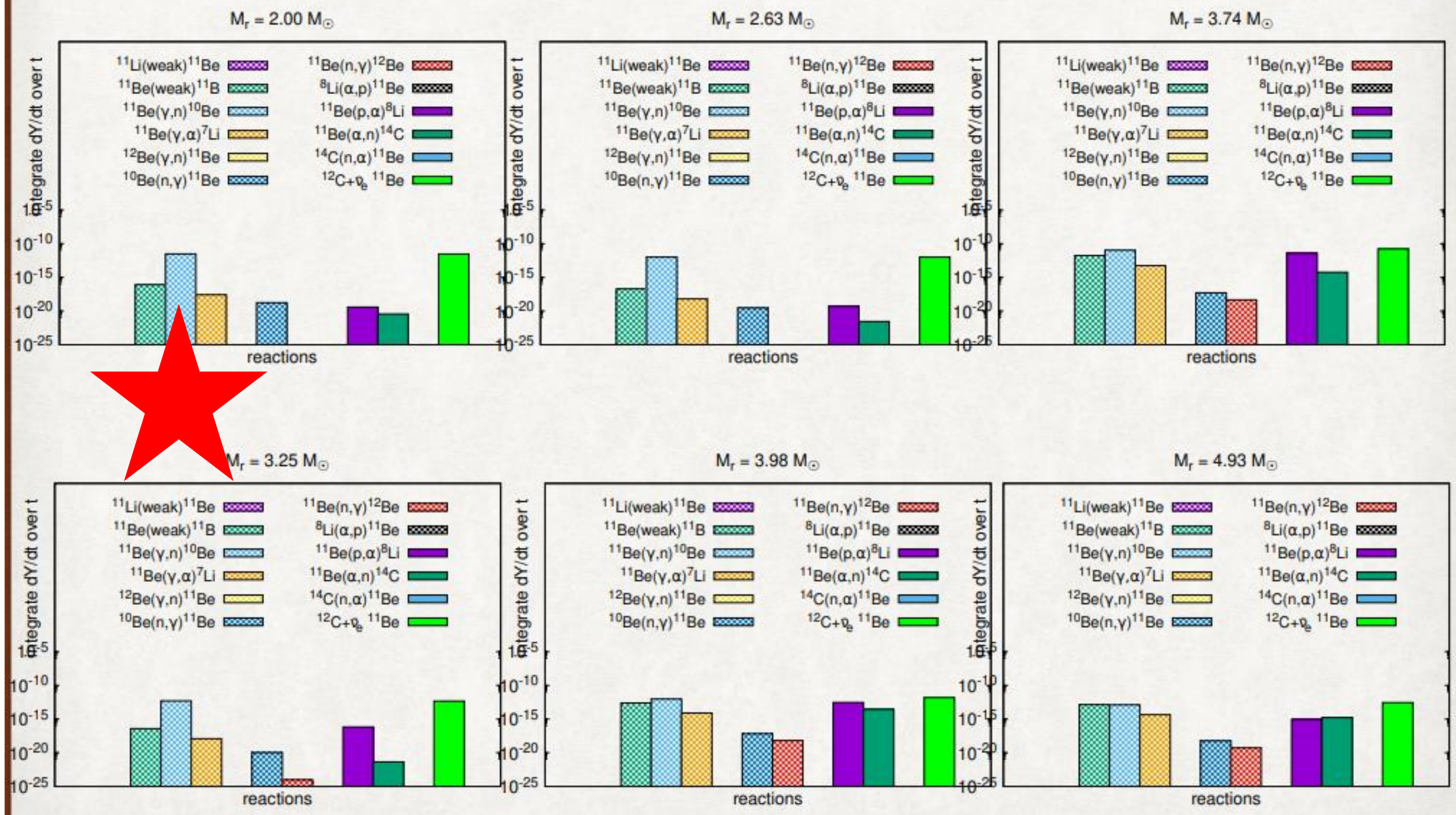

Why $^{11}Be(\gamma,n)^{10}Be$ is so high?

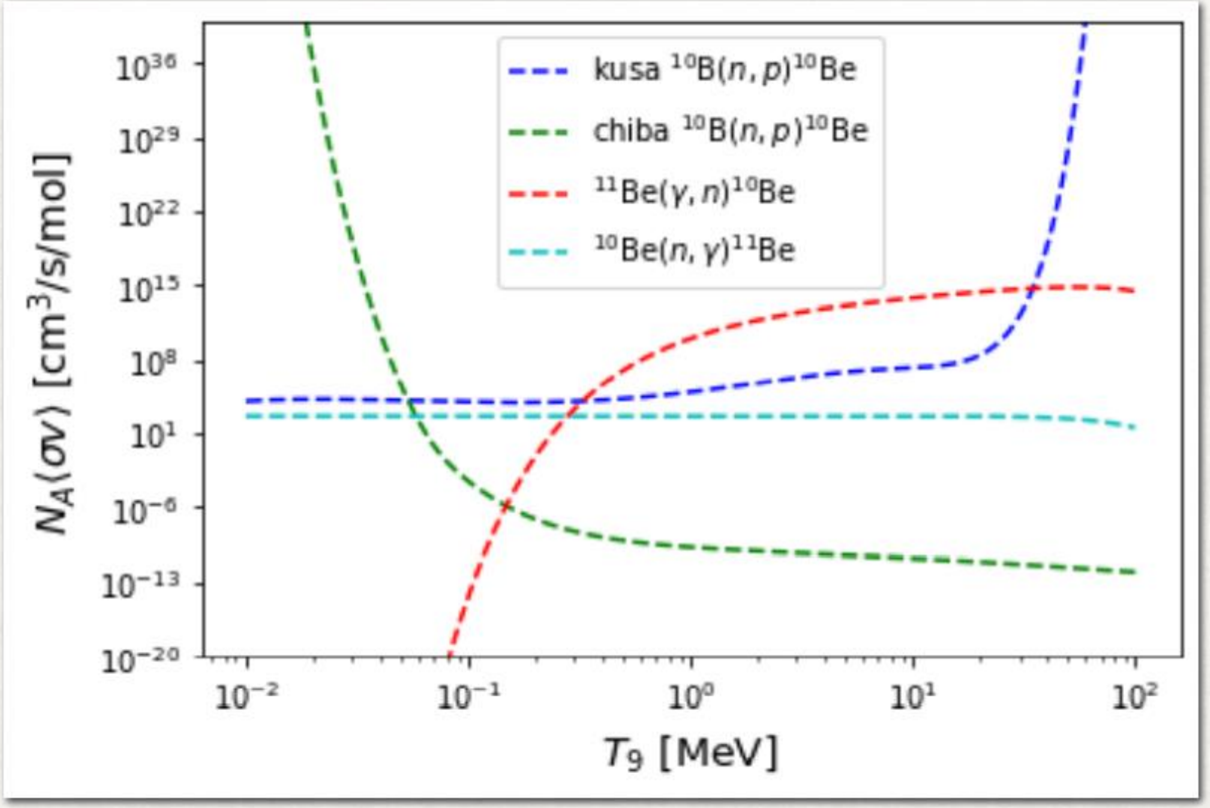

We used the (n,g) data from NNDC and calculated reverse reaction by the balance equation.
The contribution turns out to be critical for the 10Be production process.
Of course, we need experimental data to justify these reactions.

1. Motivation
1-1. Exotic Light Nuclei
1-2. Low Energy Nuclear Reactions (LENR) for Exotic Nuclei

2. LENR for Carbon isotopes
2-1. Quasi-elastic scattering of C isotopes — Submitted to PRC (2022)
2-2. 12C + 12C scattering — PRC 104, 034306 (2021)

3. LENR for 10Be — ArXiv: 2203.13365: ApJS, in press, (2022)
3-1. Cosmological Origin of 10Be
3-2. Elastic and non-elastic scattering

EPJA 56, 42 (2020), LRN for 197Au
PRC 92, 014627 (2015) LRN potential
PRC 92, 044618 (2015) LRN potential
PRC 93, 954624 (2016) Radius

Exotic structure of ^{11}Be

◆ Parity inverted ground state of the $^{11}_{4}Be_7$

- **The ground state of ^{11}Be is the $1/2^+$,**
  while ordinary nuclei have a $1/2^-$ state as the ground state
  ⟶ Vanishing of the magic number N=8

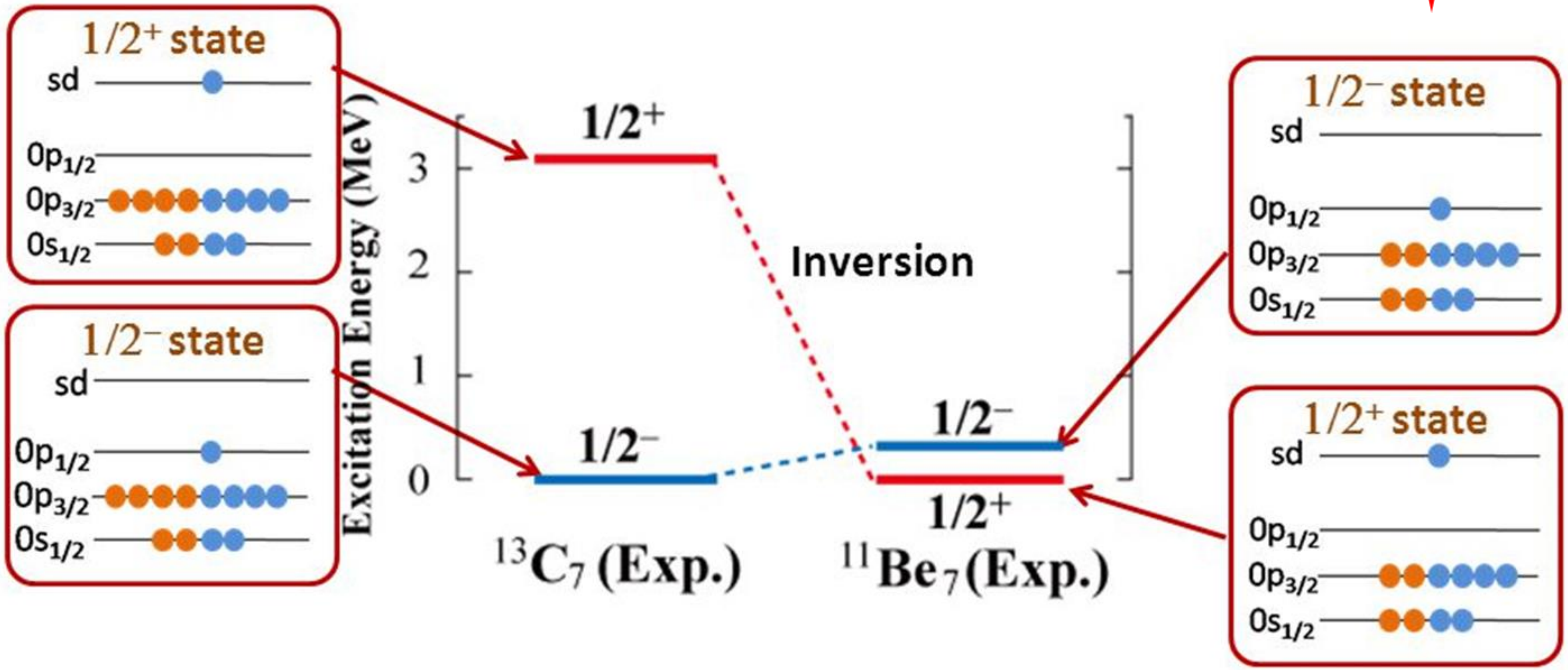

Dynamics of Halo Nuclei

Optical model potential

Complex optical model potential (for $^{10}\mathrm{Be}$)

$$-U_{\mathrm{OM}}^{10\mathrm{Be}} = -U_C(r) + [V_0^{sh}(r) + iW_0^{sh}(r)]$$

$$* \mathrm{R_i} = \mathrm{r_i}\left(A_T^{\frac{1}{3}} + A_P^{\frac{1}{3}}\right)$$

$$* r_c = 1.25$$

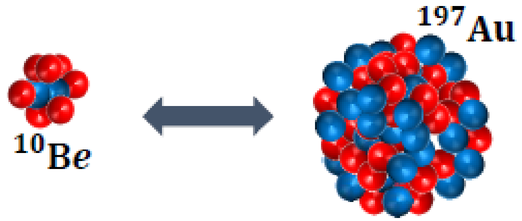

$$V_0^{sh}(r) = V\{\frac{1}{1 + \mathrm{e}^{(\mathrm{r}-R_V)/a_V}}\}$$

$$W_0^{sh}(r) = W\{\frac{1}{1+\mathrm{e}^{(\mathrm{r}-R_W)/a_W}}\}$$

$$U_C(r) = \frac{Z_p Z_T e^2}{R_c} \qquad \text{For } r > R_c$$

$$= \frac{Z_p Z_T e^2}{R_c}\left(\frac{3}{2} - \frac{1}{2}\frac{r^2}{R_c^2}\right) \qquad \text{For } r < R_c$$

The Extended optical potential(for $^{11}\mathrm{Be}$)

$$-U_{\mathrm{OM}}^{11\mathrm{Be}}(\mathrm{r}) = U_{\mathrm{OM}}^{10\mathrm{Be}} + U_0^{lo}$$

$$= U_{\mathrm{OM}}^{10\mathrm{Be}} + \{U_{CDE} + U_{LRN}\}$$

$$= U_{\mathrm{OM}}^{10\mathrm{Be}}(r) + [\{U_{CDE}^{br}(r) + U_{CDE}^{inel}(r)\} + U_{LRN}(r)]$$

Dynamic Polarization Potential

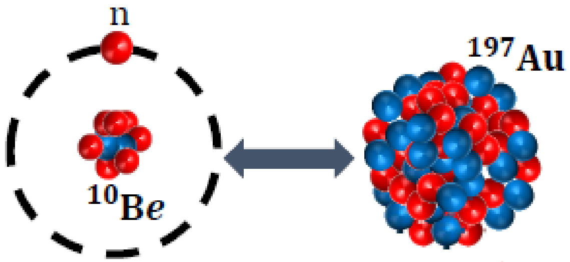

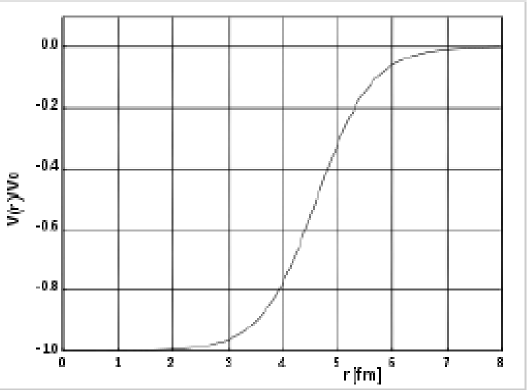

Woods–Saxon potential for A = 50, relative to V_0 with a = 0.5 fm

https://en.wikipedia.org/wiki/Woods%E2%80%93Saxon_potential

Long Range Nuclear (LRN) Force rather than CDE !!

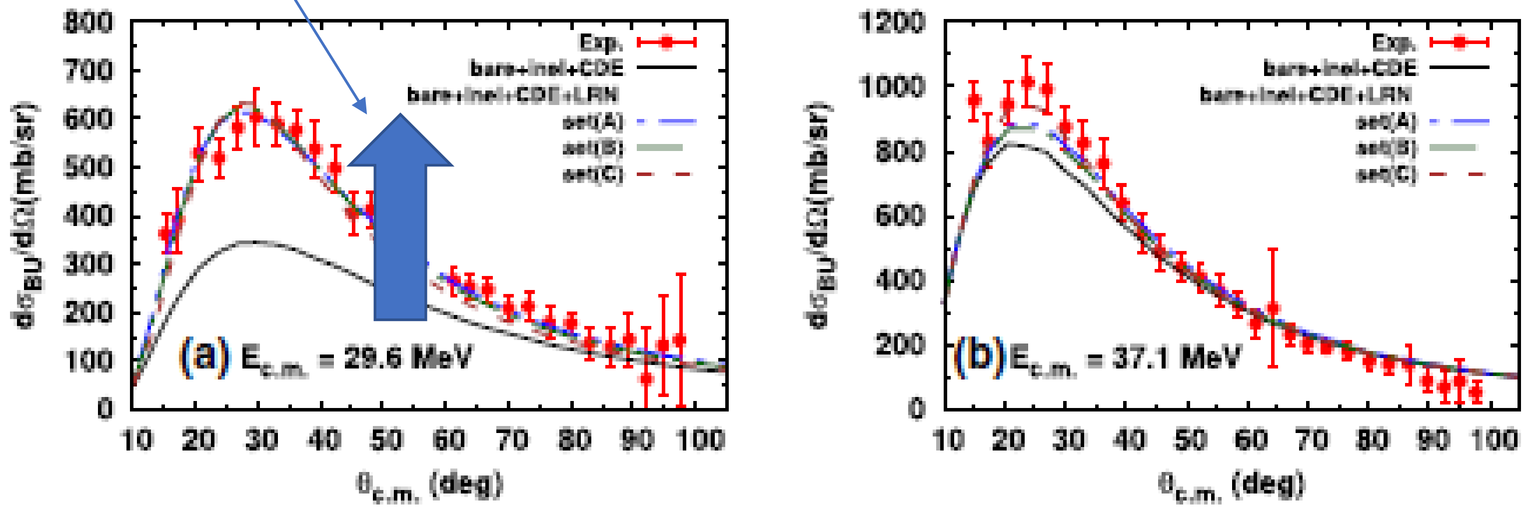

Fig. 3 (Color online) Measured break-up cross-section of the ^{11}Be + ^{197}Au system at $E_{c.m.} = 29.6$ MeV (a) and at $E_{c.m.} = 37.1$ MeV (b). The experimental data are taken from Ref. [22]. W^{br}_{CDE} means the cross-sections with the break-up channel part in the CDE potential exclusively

Coulomb Dipole Excitation Potential

M. V. Andres et al.,NPA.579.273-294(1994)

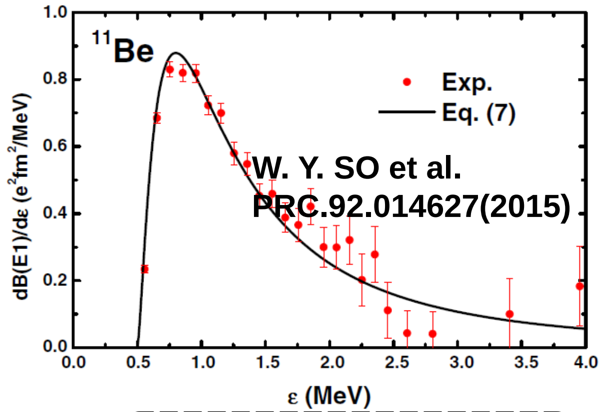

$$\boxed{\frac{dB(E1)}{d\varepsilon} = N\frac{\sqrt{\varepsilon_b}(\varepsilon-\varepsilon_b)^{3/2}}{\varepsilon^4}}$$

Unbound

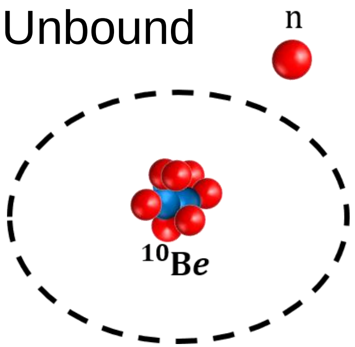

$$U_{CDE}^{br}(r) = V_{CDE}^{br}(r) + iW_{CDE}^{br}(r)$$

$$= \frac{4\pi}{9}\frac{Z_t^2 e^2}{\hbar v}\frac{1}{(r-a_0)^2 r}\int_{\varepsilon_b}^{\infty} d\varepsilon \frac{dB(E1)}{d\varepsilon} \times \left[g\left(\frac{r}{a_0}-1,\xi\right) + if\left(\frac{r}{a_0}-1,\xi\right)\right]$$

Bound

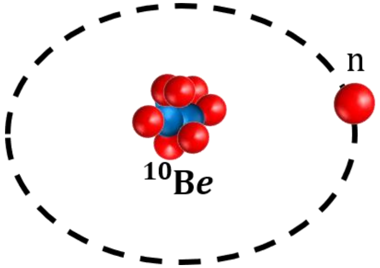

$$U_{CDE}^{inel}(r) = V_{CDE}^{inel}(r) + iW_{CDE}^{inel}(r)$$

$$= \frac{4\pi}{9}\frac{Z_t^2 e^2}{\hbar v}\frac{B(E1;\varepsilon_x^{1st})}{(r-a_0)^2 r} \times \left[g\left(\frac{r}{a_0}-1,\xi\right) + if\left(\frac{r}{a_0}-1,\xi\right)\right]$$

$*\ \varepsilon_X^{1st} = 0.32\ MeV$
$*\ \varepsilon_b$ is equal to the separation energy $S_n =$ 0.5 MeV
$*\ N = 3.1$ is the proportional constant
$*\ dB(E1)/d\epsilon$ is the Coulomb strength distribution.

$$*\ if\left(\frac{r}{a_0}-1,\xi\right) = 4\xi^2\left(\frac{r}{a_0}-1\right)^2 e^{-\pi\xi}K_{2i\xi}''\left[2\xi\left(\frac{r}{a_0}-1\right)\right]$$

$$*\ g\left(\frac{r}{a_0}-1,\xi\right) = \frac{P}{\pi}\int_{-\infty}^{\infty}\frac{d\xi'}{\xi-\xi'}f\left(\frac{r}{a_0}-1,\xi'\right)$$

$$*\ \xi = a_0\varepsilon/\hbar v,\quad a_0 = Z_p Z_t e^2/2E_{cm}$$

Elastic Scattering Cross- section

Kyoungsu Heo et al. EPJA. 56:42 (2020)

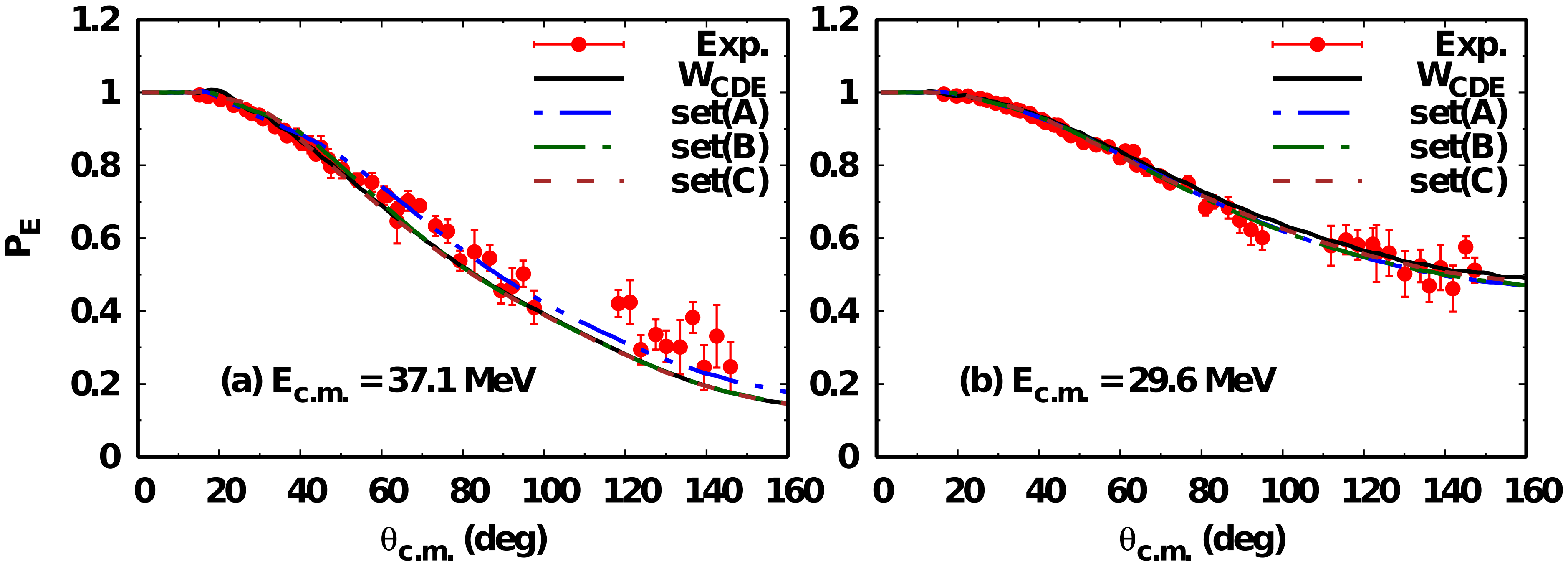

$$P_E = \ d\sigma_{el.}/d\sigma_{Ruth}$$

Inelastic Scattering Cross- section

Kyoungsu Heo et al. EPJA. 56:42 (2020)

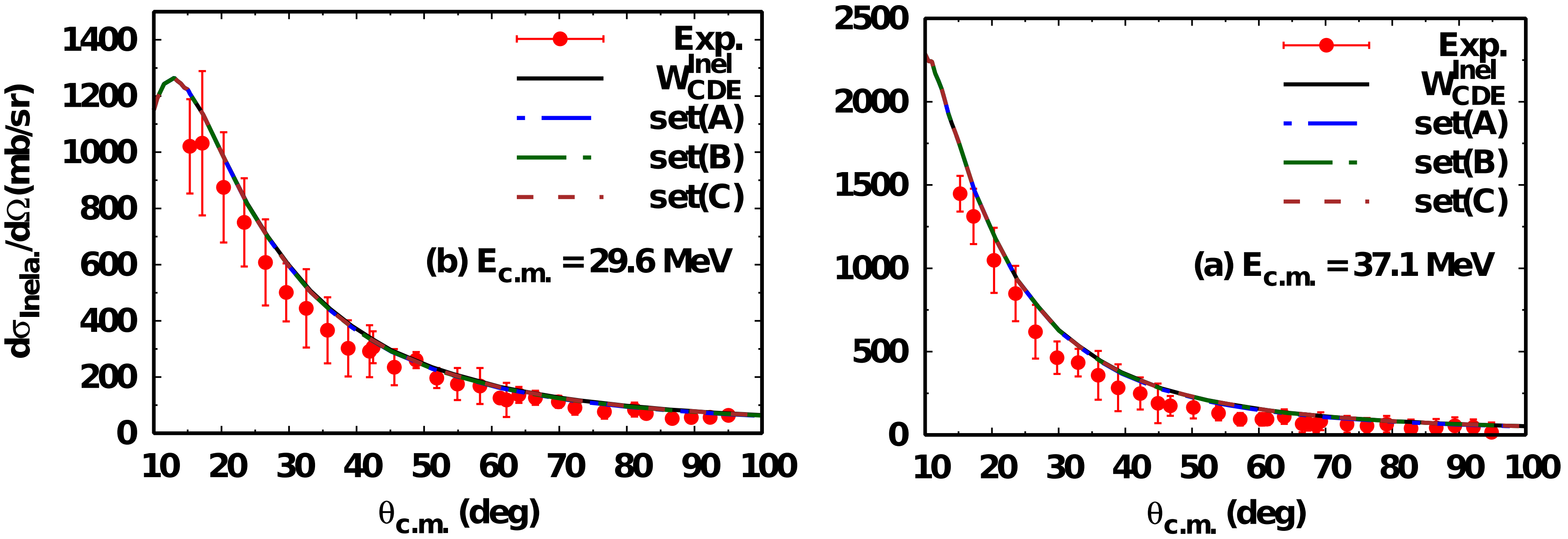

$$T_{inel;l} = \frac{8}{\hbar v}\int_0^\infty |\chi_l^+(r)|^2 [W_{CDE}^{inel}] dr$$

1. Motivation
1-1. Exotic Light Nuclei
1-2. Low Energy Nuclear Reactions (LENR) for Exotic Nuclei

2. LENR for Carbon isotopes
2-1. Quasi-elastic scattering of C isotopes
2-2. 12C + 12C scattering

3. LENR for 10Be
3-1. Cosmological Origin of 10Be
3-2. Elastic and non-elastic scattering

4. LENR 17F and 17O for mirror nuclei

5. LENR for Li and 6He isotopes and Fusions

6. Summary and Conclusion

Submitted to PRC (2022)

PRC 104, 034306 (2021)

ArXiv: 2203.13365: ApJS, in press, (2022)

EPJA 56, 42 (2020), LRN for 197Au
PRC 92, 014627 (2015) LRN potential
PRC 92, 044618 (2015) LRN potential
PRC 93, 954624 (2016) Radius

PRC 105, 014601 (2022)

PRC 89, 057601 (2014) 11Li
PRC 90, 054615 (2014) 11Li
PLB 780, 455 (2018) Fusion
JKPS 70, 42 (2017) Fusion
PRC 103, 034611 (2021) Fusion

Summary and Conclusion

1. For the ratio of the X-section to Rutherford scattering of Carbon isotopes, specifically, for 10C, we construct the BU potential and explained the irregular behavior of 10C scattering.

2. In order to understand the dominant role of IS(T=0, np) part in the two nucleon knockout reactions of 12C + 12C scattering, we explicitly include the TF in the residual interaction inside nuclei and explain the large ratio of the IS to IV (nn and pp) knockout reactions.

3. For understanding the cosmological origin of 10Be, we examine the thermal nuclear reactions for the production mechanism. 10Be(p,a)13C, **10Be(n,p)10B, 10B(p,n)10Be** turn out to play crucial roles as well as the neutrino-induced reactions on 12C.
In addition, **11Be(g,n)10B** reaction is suggested to be another key reaction to explain the meteorite abundance ratio.

4. For LENR of 11Be, we calculated the BU reaction, the inelastic scattering by the CDE and finally explained the ratio of the quasi-elastic scattering.

5. For other halo nuclei, such as 11Li and 6He, we can explain the X-section data by the OM or extended OM approach. For detailed calculations including fusion reactions, we refer to the references of our previous papers.

Thanks for your attention !!